

Review

Dark Matter Searches with Top Quarks

J. Katharina Behr ^{*,†}  and Alexander Grohsjean ^{*,†} 

Deutsches Elektronen-Synchrotron DESY, Notkestr. 85, 22607 Hamburg, Germany

* Correspondence: katharina.behr@desy.de (J.K.B.); alexander.grohsjean@desy.de (A.G.)

† These authors contributed equally to this work.

Abstract: Collider signatures with top quarks provide sensitive probes of dark matter (DM) production at the Large Hadron Collider (LHC). In this article, we review the results of DM searches in final states with top quarks conducted by the ATLAS and CMS Collaborations at the LHC, including the most recent results on the full LHC Run 2 dataset. We highlight the complementarity of DM searches in final states with top quarks with searches in other final states in the framework of various simplified models of DM. A reinterpretation of a DM search with top quarks in the context of an effective field theory description of scalar dark energy is also discussed. Finally, we give an outlook on the potential of DM searches with top quarks in LHC Run 3, at the high-luminosity LHC, and possible future colliders. In this context, we highlight new benchmark models that could be probed by existing and future searches as well as those that predict still-uncovered signatures of anomalous top-quark production and decays at the LHC.

Keywords: top quark; dark matter; WIMP; LHC



Citation: Behr, J.K.; Grohsjean, A. Dark Matter Searches with Top Quarks. *Universe* **2023**, *9*, 16. <https://doi.org/10.3390/universe9010016>

Academic Editors: Efe Yazgan, Pedro Ferreira da Silva and Jinmin Yang

Received: 18 November 2022

Revised: 16 December 2022

Accepted: 20 December 2022

Published: 27 December 2022



Copyright: © 2022 by the authors. Licensee MDPI, Basel, Switzerland. This article is an open access article distributed under the terms and conditions of the Creative Commons Attribution (CC BY) license (<https://creativecommons.org/licenses/by/4.0/>).

1. Introduction

The particle nature of dark matter (DM) is one of the major puzzles in modern particle physics, despite long-standing evidence for its existence. As early as 1884, Lord Kelvin realized that the mass of the Milky Way derived from the velocity dispersion of the stars orbiting its center is very different from the mass of the visible stars. He considered the majority of stars in our galaxy to be dark bodies. One hundred and forty years later, overwhelming astronomical and cosmological evidence has been accumulated for the existence of dark matter (DM) across different scales, ranging from the rotational velocity of stars in ultra-faint galaxies over gravitational lensing effects to precision measurements of the cosmic microwave background [1–5].

It is well established that 85% of the matter in our Universe consists of DM. The dominant part of DM must be stable with a lifetime much longer than the age of the Universe. The fact that DM was already produced in the early Universe may provide a clue to nongravitational interactions. At the same time, the feature that DM must form cosmological structures consistent with current observations allows setting a limit on the strength of DM interactions with SM particles and with itself. It is clear that none of the Standard Model particles is consistent with all of these observations.

One of the highly-motivated theory paradigms for DM is the so-called WIMP (weakly interacting massive particle) paradigm, also known as the WIMP miracle [6]. Assuming DM to be produced via the freeze-out mechanism, one can achieve the observed relic density when the DM mass is close to the electroweak scale and when the DM coupling to Standard Model particles is on the order of the weak interaction. Consequently, DM particles could be produced and studied at the Large Hadron Collider (LHC) [7]. Alternative strategies to search for DM include *indirect detection* searches, which target recoils of DM particles from the local DM halo in sensitive underground detectors, as well as *indirect detection* searches, which aim to detect the products of DM interactions, such as DM annihilation

into SM particles, e.g., gamma rays, within the visible universe. Recent reviews of results from direct- and indirect-detection searches can be found in Refs. [8,9], respectively.

An advantage of DM searches at colliders, besides the fact that DM would be produced under controlled experimental conditions, lies in the fact that they could provide access to the particles mediating the interactions between DM and the Standard Model. A DM mediator produced in proton–proton (pp) collisions could decay to DM particles. Such *invisible decays* could only be inferred via the presence of missing transverse momentum, p_T^{miss} , in the detector. However, a DM mediator decaying back into SM particles (*visible decays*) would provide direct access to its properties. DM searches at the LHC explore both avenues. To detect the invisible decays of a mediator, it is mandatory to produce the mediator in association with SM particles. In this review article, we will focus on the associated production with top quarks and, more generally, on the role of top quarks in the quest for DM. Best suited to study DM in top-quark channels are the two general-purpose detectors ATLAS [10] and CMS [11]. Recent reviews of DM searches at the LHC, including those without top quarks, can be found, e.g., in Refs. [12,13].

Discovered in 1995 at the Fermilab Tevatron collider [14,15], the top quark is the heaviest of all known elementary particles. In the case of a DM mediator with Yukawa-like couplings, the top quark would be ideal for discovery. Moreover, the top quark would allow for a first characterization of the dark sector. Due to its short lifetime, the top quark fully transmits its spin information to the decay particles. In turn, this allows inferring the spin of the mediator for both the associated production of top quarks and DM as well as for the decay of a mediator to a top-quark pair.

Another major unknown in the physics of our universe, besides the particle nature of DM, is the origin of its accelerating expansion [16,17], which is usually attributed to the presence of a yet-unknown repulsive force, referred to as dark energy (DE). If DE is a scalar field, it may be possible to produce it at the LHC. Similar to DM, DE would escape the detector unnoticed. DM searches with top quarks could be sensitive to DE production, as shown in Sections 2.4 and 4.4 of this review.

This article is structured as follows. After a detailed discussion of the underlying DM models in Section 2, we focus on the experimental signatures of DM searches involving top quarks at LHC in Section 3. In Section 4, current highlights and results from DM searches at LHC are summarized. We conclude with a discussion of uncovered signatures and models, followed by an outlook on prospects for discovering DM at future colliders in Sections 5 and 6.

2. Models with BSM Signatures Involving Top Quarks

Collider searches for DM are usually interpreted in the context of so-called *simplified models*, which contain a minimal set of new particles and couplings. Most of these models contain only a single Dirac DM particle and a single mediator particle. They are characterized by a minimal set of free parameters, namely, the masses of the DM and mediator particles and the couplings of the mediator to the SM and dark sector. Simplified models provide a convenient framework to compare searches in different final states and among different experiments. In the following, the simplified models used for the interpretation of DM searches involving top quarks are described. Additionally, an effective field theory (EFT) description of scalar DE is introduced.

2.1. Vector and Axial-Vector Mediators

2.1.1. Flavor-Conserving Interaction

A mediator with flavor-universal couplings to the SM quarks and leptons, respectively, is predicted in a simplified model that describes a flavor-conserving interaction between a fermionic WIMP DM particle χ and the SM fermions [18]. It is based on a simple extension of the SM by a new $U(1)$ gauge symmetry under which χ , as well as some of the SM fermions, are charged, thus allowing the mediator to couple to the SM sector. The interaction described by this gauge group is mediated by the s -channel exchange of a new,

electrically neutral spin-1 particle Z' with either vector or axial-vector couplings to the DM and SM fields. It is referred to as *vector mediator* or *axial-vector mediator* in the following.

The model contains five free parameters [18]: the masses of the mediator, $m_{Z'}$, and the DM particle, m_χ , as well as the quark-flavor universal coupling g_q of the mediator to quarks, the lepton-flavor universal coupling g_ℓ of the mediator to leptons, and the coupling g_χ of the mediator to DM.

The mediator can decay either invisibly into a $\chi\bar{\chi}$ pair or visibly into a fermion–anti-fermion $f\bar{f}$ pair, as illustrated schematically by the left and right diagrams, respectively, in Figure 1. The former process can be detected as a $p_T^{\text{miss}} + X$ signature in the presence of initial-state radiation (ISR), where X can be a gluon, photon, or vector boson, depending on the type of ISR, while the latter process results in a resonant enhancement in the invariant mass spectrum of the $f\bar{f}$ pair.

Constraints on this model are derived in various parameter planes, including the $(m_{Z'}, m_\chi)$ plane for fixed couplings g_q, g_ℓ, g_χ [19] and as upper limits on g_q as a function of $m_{Z'}$, as shown in Section 4.1.1.

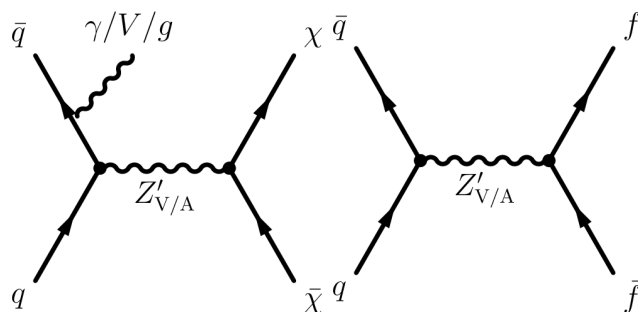


Figure 1. Schematic representation of the dominant production and decay modes of the simplified model with an s-channel vector or axial-vector mediator Z' [19].

2.1.2. Flavor-Changing Interaction

DM signatures with top quarks are predicted in simplified models containing a vector mediator Z'_{VFC} with a flavor-changing coupling V_{ut} to the top and up-quark. This type of model, referred to as *VFC model* in the following, is motivated, for example, by scenarios with DM in a hidden sector that only interacts with the SM sector via a flavor-changing coupling of a Z' boson [20,21]. The dominant production and decay modes of the VFC model are shown in Figure 2. The mediator can be produced on-shell in association with a single top or anti-top (left diagram) and decay either invisibly into DM or visibly into a top and up-quark. The former decay results in a $p_T^{\text{miss}} + t$ signature, often referred to as *mono-top*. The latter decay yields a characteristic final state with two top quarks (tt) or two anti-top quarks $\bar{t}\bar{t}$ (same-sign tt). This signature can be easily distinguished from the more abundant $t\bar{t}$ production via SM processes by the sign of the lepton charges in fully leptonic decays. Similar $tt/\bar{t}\bar{t}$ final states arise from the other two diagrams in Figure 2, which represent the t -channel exchange of the Z'_{VFC} mediator.

The VFC model is fully characterized by four free parameters: the mass of the mediator, $m_{Z'_{\text{VFC}}}$, the mass of the DM particle, m_χ , the coupling of the mediator to DM, g_χ , and the flavor-changing coupling, g_{ut} [22]. The DM mass has no significant impact on the collider phenomenology of the VFC model, if $2m_\chi < m_{Z'_{\text{VFC}}}$, and is fixed to a value of 1 GeV for existing collider searches [19]. Constraints on the VFC model are accordingly derived in several parameter planes involving the remaining free parameters (or dependent parameters): $m_{Z'_{\text{VFC}}}, g_{ut}$, and the invisible branching ratio $\mathcal{BR}(\chi\bar{\chi})$ of the mediator.

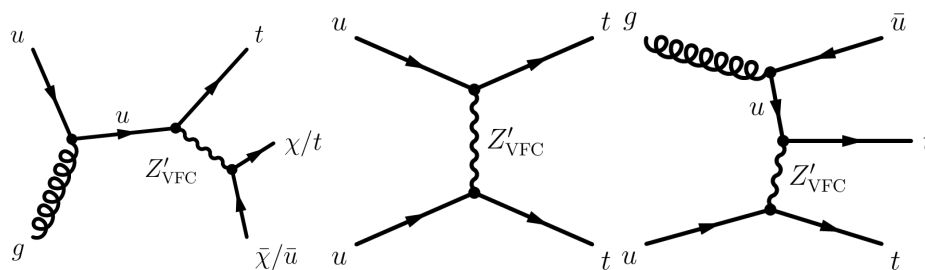


Figure 2. Schematic representation of the dominant production and decay modes of the VFC model [19].

2.2. Scalar and Pseudoscalar Mediators

A preferred coupling of DM to top quarks is predicted in simplified models containing a spin-0 mediator with Yukawa-like couplings to SM fermions. The mediator can be either a scalar (ϕ) or pseudoscalar (a). These models can be straightforwardly embedded in ultraviolet (UV) complete theories with extended Higgs sectors, such as two-Higgs-doublet models (2HDMs; see also Section 2.3). Assuming Yukawa-like couplings allows this class of models to satisfy strong constraints from flavor precision measurements. The dynamics of flavor violation are completely determined by the structure of the ordinary fermion Yukawa couplings, which is referred to as *minimal flavor violation (MFV)* [23].

The simplified models described in this section can be broadly categorized into models with a color-neutral and a color-charged interaction. An overview of the models falling into each category can be found in Ref. [19] and references therein. Two representative benchmark models used by the ATLAS and CMS collaborations are presented in the following.

2.2.1. Color-Neutral Interaction

A color-neutral interaction between an SM and a DM particle is described by a simplified model with a neutral, scalar, or pseudoscalar mediator [18,24] with Yukawa-like couplings to the SM fermions. The model has four free parameters: the mass of the DM particle, m_χ , the mass of the mediator, $m_{\phi/a}$, the coupling of the mediator to DM, g_χ , and the coupling of the mediator to SM fermions. The latter is parameterized by a flavor-universal coupling constant $g_q \equiv g_u = g_d = g_\ell$, which modifies the SM-like Yukawa coupling of the mediator to fermions [24], thus satisfying the requirements of MFV. It should be noted that couplings to leptons are explicitly included in the model, but in practice, the related signatures play no significant role in the parameter space accessible to collider searches [18]. Couplings to vector bosons W, Z are not included in this simplified model [24]. The Yukawa-like couplings imply that the mediator is mostly produced via loop-induced gluon fusion via a heavy-quark dominated loop or in association with heavy-flavor quarks, mostly top quarks. Additionally, visible decays of the mediator preferentially result in heavy quarks. The dominant production and decay modes of the mediator with heavy-flavor quarks in the final state are shown in Figure 3. These are (from left to right):

- Visible decay of a mediator produced via gluon-fusion to heavy-flavor quarks, resulting in a resonant $t\bar{t}$ or $b\bar{b}$ signal.
- Associated production of a mediator that decays either visibly or invisibly with heavy-flavor quarks, leading to a $p_T^{\text{miss}} + t\bar{t}/b\bar{b}$ signature in the case of invisible mediator decay or characteristic fully visible $t\bar{t}t\bar{t}$, $t\bar{t}b\bar{b}$, $b\bar{b}b\bar{b}$ signatures.
- Associated production of an invisibly decaying mediator with a top quark and a light (d, u, s, c) quark, leading to a $p_T^{\text{miss}} + tj$ signature.
- Associated production of an invisibly decaying mediator with a top quark and a W boson, resulting in a $p_T^{\text{miss}} + tW$ signature.

Additional signatures not shown here include $p_T^{\text{miss}} + \text{jet}$ and $p_T^{\text{miss}} + V/h$ production.

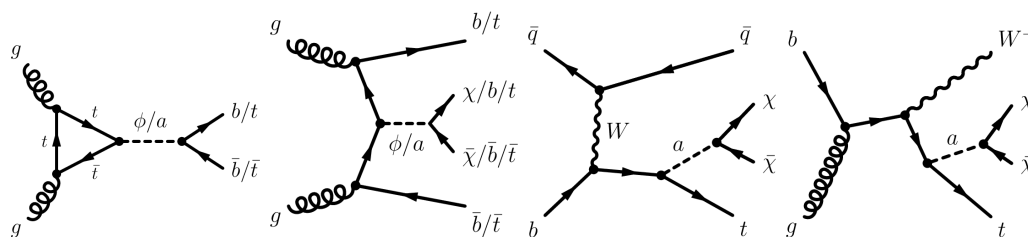


Figure 3. Schematic representation of the dominant production and decay modes with heavy-flavor quarks in the final state in the simplified model with a scalar (ϕ) or pseudoscalar (a) mediator [19].

It should be noted that, while the Yukawa-like coupling structure implies a greater importance of signatures involving top quarks rather than bottom quarks in the final state, signatures involving bottom quarks are still relevant as some UV completions of this simplified model involve a parameter modifying the relative importance of the couplings to up- and down-type quarks. In these UV completions, signatures involving bottom quarks can be more sensitive than signatures involving top quarks if the couplings to up-type quarks are suppressed.

2.2.2. Color-Charged Interaction

A color-charged interaction between the SM quarks and DM is described in a class of simplified models containing a scalar, color-triplet mediator particle. This type of simplified models is inspired by the minimal supersymmetric standard model (MSSM) [25,26] with first- and second-generation squarks and neutralino DM [19]. The mediator couplings to quarks and DM in the simplified models, however, can differ from those of the MSSM, leading to additional production diagrams.

Different models of color-charged mediators, differing by the mediator couplings to quarks, have been probed at the LHC. These include a model with preferred couplings of the mediator to the first and second quark generation, a model with preferred mediator couplings to bottom quarks, and a model with preferred mediator couplings to top quarks. Only the latter will be discussed in this review. The concrete realization of this model is documented in Ref. [21]. It contains a new $SU(2)_L$ singlet field that couples to right-handed quarks. The mediator corresponding to this field is produced from a down-type quark–anti-quark pair and decays to a top quark and a DM particle, as illustrated in Figure 4. This model can be related to the MSSM if an additional R-parity violating interaction of the top squark with the down-type quarks is assumed [19]. The free parameters of this model are the mass of the DM particle, m_χ , the mass of the mediator, m_{η_t} , the t -DM coupling strength of the mediator, λ_t , and the coupling strength of the mediator to down-type quarks, g_{ds} .

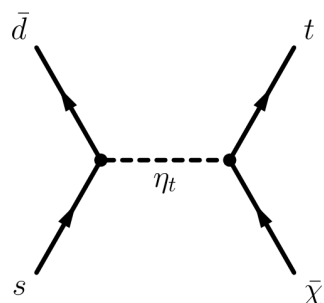


Figure 4. Schematic representation of $p_T^{\text{miss}} + t$ production via a color-changing scalar mediator η_t [19].

2.3. Extended Higgs Sectors

Extended Higgs sectors are predicted by a range of BSM theories, such as supersymmetry [27], certain classes of axion models [28], or theories predicting additional sources of CP violation in the Higgs sector to explain the observed baryon asymmetry in the universe [29,30]. Extension of the SM Higgs sector by a second complex $SU(2)$ doublet,

referred to as two-Higgs-doublet models (2HDMs), are among the simplest and most studied models with an extended Higgs sector, historically due to their strong motivation from supersymmetry. In the past years, 2HDMs have also received considerable attention from the DM community as a means of embedding the simplified, mediator-based, models described in the previous sections in the context of a UV-complete and renormalizable framework with a broader collider phenomenology. Models of DM based on a 2HDM with a vector [31], pseudoscalar [32,33], and scalar [34] mediator have been proposed. Concrete realizations of the former two have been used as benchmark models by the LHC experiments. Models with vector mediators are not discussed in this review as final states with top quarks do not play a dominant role in their phenomenology. Models with a pseudoscalar mediator, on the other hand, feature a rich phenomenology involving relevant signatures with top quarks due to the Yukawa-type coupling of the mediator to SM fermions. Pseudoscalar mediators are also particularly interesting to study at the LHC as they are not strongly constrained by direct-detection experiments because the DM–nucleon scattering cross-section pseudoscalar couplings are strongly suppressed at tree-level by the momentum transfer in the nonrelativistic limit [35]. A concrete realization of a 2HDM with a pseudoscalar mediator that is used as a benchmark model by the LHC experiments is described in Section 2.3.

2HDM with a Pseudoscalar Mediator

A 2HDM with a pseudoscalar mediator a [32], referred to as 2HDM + a in the following, is a more complex simplified model that embeds the phenomenology of the simplified models with a color-neutral pseudoscalar mediator (Section 2.2.1) in more complete model with a second complex SU(2) doublet. The 2HDM in this model has a CP-conserving potential with a softly broken \mathbb{Z}_2 symmetry [36]. Its Higgs sector contains five Higgs bosons: two scalars, h and H , a pseudoscalar, A , and two charged Higgs bosons H^\pm . The alignment limit is assumed, meaning that one of the two scalars of the model is identified with the 125 GeV Higgs boson discovered in 2012. Furthermore, the Yukawa structure of the 2HDM is of type-II [37], meaning that couplings of the additional Higgs bosons to top quarks are preferred over those to other fermions at low values of the ratio of the two vacuum expectation values, $\tan\beta$, one of the model parameters with the biggest impact on the collider phenomenology of the model. The pseudoscalar mediator a mixes with the pseudoscalar A of the 2HDM with mixing angle θ .

The phenomenology of the 2HDM + a is fully defined by 14 free parameters, making it considerably more complex than the simplified models described in the previous sections. These parameters are as follows: the masses m_h , m_H , and m_A of the neutral Higgs bosons; the masses m_{H^\pm} of the charged Higgs bosons; the mass m_a of the mediator; the mass m_χ of the DM particle; the coupling y_χ between DM and the mediator; the three quartic couplings λ_{P1} , λ_{P2} , λ_3 of the mediator to the SU(2) fields; the vacuum expectation value (VEV) v of the electroweak sector; the ratio $\tan\beta = \frac{v_2}{v_1}$ of the VEVs of the two Higgs fields; the mixing angle α between the two scalar Higgs bosons h and H ; and the mixing angle θ between the pseudoscalar Higgs boson A and the mediator a .

The choice of the alignment limit ($\cos(\beta - \alpha) = 0$) implies that $m_h = 125$ GeV and $v = 246$ GeV. The DM–mediator coupling is set to unity ($y_\chi = 1.0$) without significant impact on the phenomenology of the model. The setting $\lambda_3 = 3$ is chosen to ensure the stability of the Higgs potential in the mass ranges of interest of the heavy Higgs bosons [19]. Furthermore, the choice $\lambda_{P1} = \lambda_{P2} = \lambda_3 = 3$ maximizes the trilinear couplings between the CP-even and CP-odd neutral states [19]. Finally, the choice $m_A = m_H = m_{H^\pm}$ ensures compatibility of the model predictions with flavor constraints [32] and additionally simplifies the phenomenology of the model [19].

With these constraints, the remaining 2HDM+ a parameter space can be described by the following five parameters: m_A , m_a , m_χ , $\sin\theta$, and $\tan\beta$. Representative benchmark scans of this parameter space have been defined by the LHC Dark Matter Working Group [38] with the aim to highlight different aspects of the phenomenology of this bench-

mark model and the interplay between searches targeting different signal processes across this parameter space. Additional benchmark scans are defined in Ref. [39].

The 2HDM + a predicts a rich phenomenology with a diverse range of final states. The dominant processes leading to final states with top quarks are shown in Figure 5, along with the leading diagrams for the resonant production of an invisibly decaying mediator with a Higgs or Z boson, leading to $p_T^{\text{miss}} + h$ and $p_T^{\text{miss}} + Z$ final states, respectively, which are among the most sensitive probes of the 2HDM + a . A full overview of the phenomenology of the 2HDM + a can be found in Refs. [32,38].

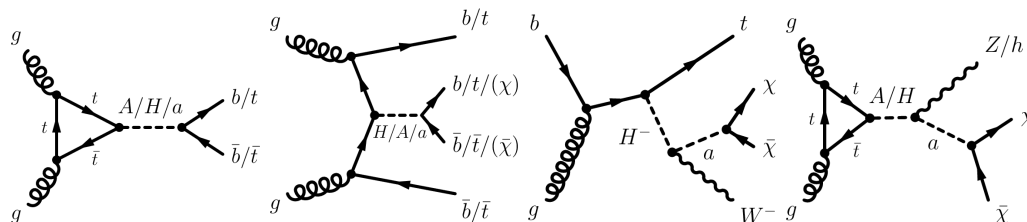


Figure 5. Schematic representation of relevant production and decay modes with top quarks leading to either top quarks in the final state or $p_T^{\text{miss}} + h/Z$ signatures. From left to right: resonant production of a neutral scalar or pseudoscalar particle $H/A/a$ decaying to $t\bar{t}$ or $b\bar{b}$; associated production with $b\bar{b}$ or $t\bar{t}$ of a single $H/A/a$ decaying either visibly to heavy flavor or invisibly to DM; associated production of a top quark and a charged Higgs boson decaying to a W boson and an invisibly decaying mediator a ; resonant A/H production with subsequent decay to a Z/h boson and an invisibly decaying mediator a [19].

2.4. EFT Model of Scalar Dark Energy

Searches for DM signatures involving top quarks provide a powerful tool to probe models of scalar DE. The first reinterpretation of DM searches in the context of DE, which relied on the analysis of 36 fb^{-1} of LHC Run 2 data [19], used an EFT implementation [40] of the Horndeski theories [41] to describe DE production at the LHC [19]. The latter introduce a new scalar field, ϕ_{DE} , corresponding to DE, that couples to gravity.

The EFT model contains two classes of operators: operators that are invariant under a shift symmetry $\phi_{\text{DE}} \rightarrow \phi_{\text{DE}} + \text{constant}$ and operators that break this symmetry. The former contain only derivative couplings of the DE field to SM fermions as direct Yukawa-type interactions break the shift symmetry. The latter induce direct couplings of the DE field to the SM fermions, such as Yukawa-type interactions, and are subject to tight experimental constraints [42].

Only shift-symmetric operators of the EFT model have been considered for the DE reinterpretation of LHC DM searches [19]. The model under consideration contains nine such operators, $\mathcal{O}_i^{(d)}$, where d denotes the dimensionality of the operator. This leads to nine possible terms in the Lagrangian, each suppressed by powers of a characteristic energy scale M_i^{d-4} , according to the operator’s dimensionality:

$$\mathcal{L} = \mathcal{L}_{\text{SM}} + \sum_{i=1}^9 c_i \mathcal{L}_i = \mathcal{L}_{\text{SM}} + \sum_{i=1}^9 \frac{c_i}{M_i^{d-4}} \mathcal{O}_i^{(d)},$$

where the c_i denote the Wilson coefficients.

Only the phenomenology of the two leading, i.e., least suppressed, terms has been considered by the LHC experiments so far. These are of dimension eight and can be expressed in terms of the conformal anomaly, $T_\nu^\nu (= m\bar{\psi}\psi$ for a Dirac field), and the energy-momentum tensor of the SM Lagrangian $T^{\mu\nu}$ as follows:

$$\mathcal{L}_1 = \frac{\partial_\mu \phi_{DE} \partial^\mu \phi_{DE}}{M_1^4} T^{\nu}_{\nu}$$

$$\mathcal{L}_2 = \frac{\partial_\mu \phi_{DE} \partial_\nu \phi_{DE}}{M_2^4} T^{\mu\nu}.$$

The coupling described by the first term, \mathcal{L}_1 , is proportional to the mass of the SM fermions to which the DE field couples, thus making collider signatures involving top quarks a sensitive probe of DE. A schematic representation of DE production at the LHC via this operator is shown in Figure 6. It describes the radiation of a pair of DE particles off a final-state top quark from SM $t\bar{t}$ production, leading to a $p_T^{\text{miss}} + t\bar{t}$ signature.

The second operator, \mathcal{L}_2 , involves derivatives of the SM fields and is therefore proportional to their momenta. Final states involving high-momentum intermediate states, of which a DE pair is radiated off, provide the best sensitivity to this operator. At a hadron collider such as the LHC, the most likely high-momentum intermediate state particles are hadronically interacting particles, such as gluons, leading to characteristic $p_T^{\text{miss}} + \text{jet}$ signatures as the smoking-gun signatures for DE production.

Constraints on the EFT model of DE have been derived using searches for both $p_T^{\text{miss}} + t\bar{t}$ (\mathcal{L}_1 term) and $p_T^{\text{miss}} + \text{jet}$ signatures [19] (\mathcal{L}_2 term). Only the former are discussed in this review.

It should be noted that additional signatures, such as $p_T^{\text{miss}} + t$ production, are predicted based on the sub-leading operators. The exploration of these additional signatures and possible reinterpretations of further DM searches in the context of DE is left to future work.

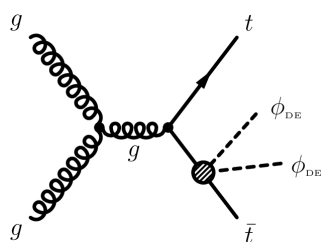


Figure 6. Schematic representation of the leading process of DE production in association with a $t\bar{t}$ pair in an EFT model of scalar DE via the operator \mathcal{L}_1 [19].

3. Experimental Signatures

Searches for DM in pp collisions involving single or multiple top quarks can be broadly split into two categories: searches for large p_T^{miss} and searches for a DM mediator decaying into SM particles. Both classes rely on different analysis techniques. Common to all searches is a detailed exploration of the top-quark decay. Due to the almost diagonal structure of the CKM matrix and, in particular, V_{tb} being close to one, the top quark decays almost 100% of the time into a bottom quark and a W boson. The W boson itself decays with about 30% probability into a charged lepton, i.e., an electron, muon, or tau, and the corresponding neutrino, or into two quarks otherwise. Similar to DM particles, neutrinos can only be inferred from missing transverse momentum in the detector. Events with two top quarks or with a single top quark and a W boson are typically categorized into three orthogonal channels based on the lepton ($\ell = e, \mu$, including decays via τ leptons, i.e., $\tau \rightarrow e, \tau \rightarrow \mu$) multiplicity in the final state. The 0-lepton (0ℓ) final states arise in events in which both W bosons decay hadronically; 1-lepton (1ℓ) final states arise in events in which one W boson decays hadronically, the other leptonically; 2-lepton (2ℓ) final states arise if both W bosons decay leptonically.

When top quarks recoil against significant p_T^{miss} or result from the decay of a very heavy resonance, top quarks are highly Lorentz-boosted and their decay products become highly collimated. In the case of hadronic top-quark decays, this means that the particle

showers from the three final-state quarks can no longer be reconstructed as three separate small-radius (small- R) jets (*resolved decay*) but instead merge into a single large-radius (large- R) jet with characteristic substructure (*merged decay*). Merged top-quark decays are identified using dedicated *top tagging* algorithms.

3.1. Final States with Invisible Decays

3.1.1. $p_T^{\text{miss}} + t$

Searches for the production of large p_T^{miss} in association with a single top quark were conducted by both the ATLAS [43] and CMS [44] collaborations.

The ATLAS Collaboration performed a $p_T^{\text{miss}} + t$ search targeting merged hadronic top-quark decays using 139 fb^{-1} of $\sqrt{s} = 13 \text{ TeV}$ pp collision data [43]. Events are required to have $p_T^{\text{miss}} > 250 \text{ GeV}$ and contain at least one large- R (anti- k_t [45] $R = 1.0$) jet with transverse momentum $350 < p_T < 2500 \text{ GeV}$ and mass $40 < m < 600 \text{ GeV}$. Additionally, the selected jet must be identified as a top-quark candidate via a dedicated top-tagging algorithm [46], which relies on a deep neural net (DNN) that uses jet kinematics and substructure variables as input [46,47]. The working point for the top tagging algorithm chosen for this analysis corresponds to a 50% top tagging efficiency.

Dedicated signal regions targeting resonant DM production via a color-charged scalar mediator (Section 2.2.2) and nonresonant DM production via a vector mediator with a V_{ut} coupling (Section 2.1.2) are defined based on the output score of XGBoost classifiers [48] that are trained on several event observables. Control regions are defined to constrain the dominant backgrounds from $t\bar{t}$ and $V + \text{jets}$ production.

A similar search was performed by the CMS Collaboration [44]. Different from the ATLAS analysis, the result is based on data recorded in 2016 that only correspond to an integrated luminosity of 36 fb^{-1} . To identify the hadronically decaying top quark, CA15 jets were used. CA15 jets are clustered from particle flow candidates using the Cambridge–Aachen algorithm [45] with a distance parameter of 1.5. The CA15 jets must have a transverse momentum $p_T > 250 \text{ GeV}$, $|\eta| < 2.4$ and an invariant mass of $110 \text{ GeV} < m < 210 \text{ GeV}$. Furthermore, several substructure observables, such as the N-subjettiness [49] or so-called energy-correlation functions [50,51], are combined in a boosted decision tree (BDT) [52] to distinguish top-quark jets from the hadronization products of single light quarks or gluons. At 50% signal efficiency, the BDT background acceptance is 4.7%. The dominant backgrounds from $t\bar{t}$ and single vector bosons (Z, W, γ) are constrained from dedicated control regions. The signal is probed in distributions of missing transverse energy p_T^{miss} considering two signal regions which correspond to a BDT output between 0.1 and 0.45 and above 0.45, respectively.

The summary plots for the benchmark model with a color-charged scalar mediator in Section 4.2.2, which show the interplay between the $p_T^{\text{miss}} + t$ and same-sign tt (Section 3.2.1) searches, are based on an earlier search of the ATLAS Collaboration using 36 fb^{-1} of $\sqrt{s} = 13 \text{ TeV}$ pp collision [53]. This analysis statistically combines the results from two orthogonal channels, targeting semi-leptonic and hadronic top-quark decays, respectively.

3.1.2. $p_T^{\text{miss}} + tW$ and $p_T^{\text{miss}} + tj$

Similar to the $p_T^{\text{miss}} + t$ searches described in Section 3.1.1, searches for $p_T^{\text{miss}} + tW$ target events with single top quarks produced in association with large p_T^{miss} additionally require the existence of a second visible object. This can be either a W boson or a hadronic jet. The resulting signatures are referred to as $p_T^{\text{miss}} + tW$ and $p_T^{\text{miss}} + tj$, respectively. It should be noted that searches in these final states are not orthogonal to the $p_T^{\text{miss}} + t$ searches discussed in Section 3.1.1, as the latter do not veto the presence of additional visible objects in the event, and hence implicitly include $p_T^{\text{miss}} + tj$ and $p_T^{\text{miss}} + tW$ signatures.

While $p_T^{\text{miss}} + t$ searches are traditionally used to constrain resonant DM production via a color-charged scalar mediator, and nonresonant DM production via a vector mediator with a flavor-violating V_{ut} coupling, as explained in Section 3.1.1, $p_T^{\text{miss}} + tW$ searches in

particular are used to probe the 2HDM + a (Section 2.3) and, more recently, also simplified models with a scalar or pseudoscalar mediator (Section 2.2.1).

Simplified models with a scalar or pseudoscalar mediator predict both $p_T^{\text{miss}} + tW$ and $p_T^{\text{miss}} + tj$ production, as illustrated by the two right-most diagrams in Figure 3. The corresponding signal cross-sections are, up to mediator masses of 200 GeV, smaller than those of the dominant $p_T^{\text{miss}} + t\bar{t}$ production mode discussed in Section 3.1.3. Therefore, $p_T^{\text{miss}} + tW$ and $p_T^{\text{miss}} + tj$ searches have not been used to constrain these simplified models by the ATLAS Collaboration. However, with the increased sensitivity of recent searches, single-top-associated production becomes more and more relevant, and a first search including $p_T^{\text{miss}} + tW$ and $p_T^{\text{miss}} + t\bar{t}$ signatures was performed by the CMS Collaboration [54], as further discussed in Section 3.1.4.

$p_T^{\text{miss}} + tW$ and $p_T^{\text{miss}} + tj$ production is also predicted in the 2HDM + a . Compared to simplified models with a single (pseudo-)scalar mediator, this model contains additional production modes, illustrated, for example, by the third diagram in Figure 5, which lead to higher predicted signal cross-sections for $p_T^{\text{miss}} + tW$ and $p_T^{\text{miss}} + tj$ production. A search for $p_T^{\text{miss}} + tW$ and $p_T^{\text{miss}} + tj$ signatures, optimized specifically for 2HDM + a signal processes, was conducted by the ATLAS Collaboration [55] using 139 fb^{-1} of $\sqrt{s} = 13 \text{ TeV}$ pp collision data. The search considers events with one or two leptons (e, μ), at least one b -tagged jet, and significant p_T^{miss} in three orthogonal categories. Two of them target $p_T^{\text{miss}} + tW$ production in final states with one or two leptons, while the third channel targets $p_T^{\text{miss}} + tj$ production in final states with exactly one lepton. The search was extended in the context of a preliminary analysis of the same dataset [56] to include events with highly energetic W boson decays in final states with zero leptons or one lepton. These provide additional sensitivity for large masses of the charged Higgs bosons. The newly added zero- and improved one-lepton channels are statistically combined with the two-lepton channel of Ref. [55].

3.1.3. $p_T^{\text{miss}} + t\bar{t}$

Searches for DM or DE production in association with a $t\bar{t}$ pair target final states characterized by sizeable p_T^{miss} and the presence of the $t\bar{t}$ decay products.

The CMS Collaboration released a search for DM in association with a $t\bar{t}$ pair using 137 fb^{-1} of data recorded at $\sqrt{s} = 13 \text{ TeV}$ between 2016 and 2018 [57]. The analysis combines previous searches in final states with 0 [58], 1 [59], or 2 [60] leptons. While the primary target of the analyses is pair production of the supersymmetric partner of the top quark ($stop$), a reinterpretation of the combined result in a simplified DM model with scalar mediators is provided.

A central feature of the analysis in the 0-lepton channel is an advanced jet-tagging algorithm identifying hadronically decaying top quarks and W bosons with low and high Lorentz-boost. For the highly Lorentz-boosted regime, the DeepAK8 algorithm [61] is used, whereas in the resolved regime the DeepResolved algorithm [59] is explored, to tag top quarks in the intermediate transverse momentum range from 150 to 450 GeV. The analysis includes a total of 183 nonoverlapping signal regions. The contribution of each SM background process is estimated through measurements of event rates in dedicated background control samples that are translated to predicted event counts in the corresponding signal region with the aid of MC simulation.

The key requirements in the 1-lepton channel are exactly one lepton and $p_T^{\text{miss}} > 250 \text{ GeV}$. Moreover, the transverse mass computed from the lepton and the missing momentum is required to be larger than 150 GeV to reduce the dominant background from SM $t\bar{t}$ and $W + \text{jets}$ production, for which the transverse mass has a natural cutoff at the mass of the W boson. The SM production of dileptonic $t\bar{t}$ events, where one of the leptons is lost, is the largest remaining background. It is estimated through a set of dedicated control regions and reduced by using the modified topness variable [59]. The 1-lepton channel also exploits the jet tagging algorithms used in the 0-lepton channel, to identify hadronic top-quark decays. In order to enhance the sensitivity to different signal scenarios, including the case of small

missing transverse momentum, events are categorized into a total of 39 nonoverlapping signal regions.

The search in the 2-lepton channel explores orthogonal signal regions based on the flavor of the leptons and three characteristic observables: the so-called missing transverse momentum significance [62] and two specific definitions of the stransverse mass [60,63]. The p_T^{miss} significance is given by the ratio of the p_T^{miss} over its resolution and it is particularly powerful to suppress events where detector effects and misreconstruction of particles from pileup interactions are the main source of missing transverse momentum. The key feature of the stransverse mass using leptons (lepton and b-quark jets) is that it retains a kinematic endpoint at the W -boson (top-quark) mass for SM background events from the leptonic decays of two W bosons (top quarks). The dominant backgrounds arise from $t\bar{t}$ and $t\bar{t} + Z$ production as well as single-top-quark production in the Wt channel. After a veto of the Z -boson mass window, i.e., $|m_{\ell\ell} - m_Z| > 15$ GeV, Drell–Yan production represents only a minor source of background.

A similar search using 139 fb^{-1} of LHC data was released by the ATLAS Collaboration exploring the 0-lepton [64], 1-lepton [65], and 2-lepton [66] channels separately. All three final states were combined afterwards into a single result [67]. In this context, the (0ℓ) channel search was further optimized through an improved selection of triggers targeting b -jets. Searches for $p_T^{\text{miss}} + tW$ (Section 3.1.2) production were not included in this combination as their datasets are not orthogonal to those in the $p_T^{\text{miss}} + t\bar{t}$ by construction. Including them in a statistical combination is left to future publications. While, by now, the $p_T^{\text{miss}} + t\bar{t}$ searches discussed above have been interpreted in simplified models with a scalar or pseudoscalar mediator only (see Section 4.2.1), earlier searches, based on smaller datasets, have already been used to constrain a 2HDM with a pseudoscalar mediator (Section 4.3.1) and a model of scalar DE (Section 2.4).

3.1.4. $p_T^{\text{miss}} + tW$, $p_T^{\text{miss}} + tj$ and $p_T^{\text{miss}} + t\bar{t}$

A first result exploring topologies of single top quark and top-quark pair associated production was released by the CMS Collaboration [54]. The analysis uses 36 fb^{-1} of data recorded in 2016 at 13 TeV and combines multiple selection categories in final states with 0 or 1 lepton. In the 1-lepton channel, dominant background is suppressed using a similar strategy as the one discussed in Section 3.1.3, while in the 0-lepton channel, dominant background is reduced by a cut on the missing transverse energy, the ratio of the leading jet transverse momentum over the total hadronic transverse energy in the event, and the minimum opening angle between the missing transverse energy and the two leading jets. To enhance the sensitivity to single top quark associated production, events are separated according to the number of identified b-quark jets. Events with a single b-tagged jet are further split into events with a central or forward jet. The categorization in terms of forward jets allows a further enhancement of $t/\bar{t} + \text{DM}$ t -channel events. This production mode leads to final states with one top quark and an additional jet, which tends to be in the forward region of the detector, while the additionally produced b-quark is typically low in transverse momentum and therefore not reconstructed. A key observation of this search is the p_T^{miss} spectrum explored in a combined fit to different orthogonal signal regions. Overall, data are found to be in good agreement with the expected SM background. Due to the combination of single top quark and $t\bar{t}$ associated production, this analysis was able to derive the most stringent limits from LHC data on spin-0 mediators at that time.

3.2. Final States without Invisible Decays

3.2.1. Same-Sign tt

Events with a same-sign tt pair are identified via the leptonic decays of the W bosons from the two top quarks. They are required to contain two same-sign charged leptons, at least one b -jet, and significant p_T^{miss} from the two neutrinos resulting from the leptonic W boson decays.

A search in same-sign $t\bar{t}$ events was conducted by the ATLAS Collaboration, using 36 fb^{-1} of $\sqrt{s} = 13 \text{ TeV}$ data [22]. The signal region of this search is defined by requiring the presence of two positively charged leptons (e, μ) and at least one b -jet. Additionally, the scalar sum of the transverse momenta of all selected objects in the event, H_T , is required to be significant ($H_T > 750 \text{ GeV}$). Further requirements on the p_T^{miss} and the angular separation of the two leptons are imposed. The signal region is split into three orthogonal channels based on the lepton flavor ($ee, e\mu, \mu\mu$). The main backgrounds of this search are estimated using MC simulation, while the subdominant background from fake leptons is estimated using data-driven techniques.

3.2.2. $t\bar{t}$

A search for resonant $t\bar{t}$ production in the 0ℓ channel was conducted by the ATLAS Collaboration using 139 fb^{-1} of $\sqrt{s} = 13 \text{ TeV}$ data [68]. This search targets heavy vector and axial-vector resonances (including DM mediators) with masses $> 1.4 \text{ TeV}$, resulting in two merged top-quark decays. Merged top-quark decays are identified using a deep neural net (DNN)-based top tagger trained on the distributions of various characteristic jet and jet substructure variables to distinguish top-quark from light-quark and gluon initiated jets. SM $t\bar{t}$ production constitutes the main, irreducible background to this search, followed by strong multijet production. The background spectrum is derived from data by fitting a smoothly falling function to the reconstructed $m_{t\bar{t}}$ distribution, similar to the approach classically chosen in di-jet resonance searches.

A larger range of resonance masses was probed by a search for resonant $t\bar{t}$ production in the 1ℓ channel, conducted by the ATLAS Collaboration on 36 fb^{-1} of $\sqrt{s} = 13 \text{ TeV}$ data [69]. This search targets both *merged* and *resolved* hadronic top-quark decays and is sensitive to resonance masses just above the $t\bar{t}$ kinematic threshold ($> 2m_{\text{top}}$). The main, irreducible background from SM $t\bar{t}$ production, as well as most other, smaller backgrounds, are estimated using MC simulation. Data-driven corrections are applied to the MC simulation of the $W + \text{jets}$ background. The small background from strong multijet production is estimated with a fully data-driven approach.

A first search for heavy spin-1 resonances combining final states with 0, 1, and 2 leptons was performed by the CMS Collaboration using data recorded at $\sqrt{s} = 13 \text{ TeV}$ and corresponding to a total integrated luminosity of 35.9 fb^{-1} [70]. The analysis utilizes reconstruction techniques that are optimized for top quarks with high Lorentz-boosts, which requires the use of nonisolated leptons partially overlapping with b -quark jets and jet substructure techniques for top-quark tagging. Except for the QCD multijet background in the 0-lepton channel, the shapes of all backgrounds are estimated from MC simulation. The signal strength is extracted from the distributions of the reconstructed invariant mass of the top-quark pair for the 0- and 1-lepton channels and from the sum of missing transverse energy and the transverse momenta of all jets and leptons in the 2-lepton channel.

Interference effects between the resonant signal and background processes are not taken into account in the searches discussed above as they are irrelevant for spin-1 and spin-2 particles. However, this is not true for scalar and pseudoscalar resonances, such as additional heavy Higgs bosons, which are produced from gg initial states via heavy quark loops. The process $gg \rightarrow A/H \rightarrow t\bar{t}$ interferes strongly with the irreducible background from SM $t\bar{t}$ production, which is dominated by $gg \rightarrow t\bar{t}$. Interference effects significantly distort the resonance lineshape from a Breit–Wigner peak to a characteristic peak-dip or even more complicated structures. The treatment of these effects is nontrivial and requires dedicated analysis methods, in particular in the statistical analysis. Searches for heavy scalars and pseudoscalars were conducted by both the ATLAS [71] and CMS collaborations [72] in the 1ℓ and $1\ell + 2\ell$ channels, respectively. These searches are sensitive to the production of scalar and pseudoscalar DM mediators; however, due to the strong model-dependence of the interference patterns, no dedicated interpretation of these results in the context of DM models exists to date. An approximate reinterpretation of the results in Ref. [71] in the context of the 2HDM + a (Section 2.3) can be found in Ref. [32].

3.2.3. $t\bar{t}\bar{t}\bar{t}$

Final states with four top quarks ($t\bar{t}\bar{t}\bar{t}$) can arise from nonresonant processes predicted in the SM but are also predicted in BSM models allowing for the associated production of a heavy BSM resonance, which subsequently decays to $t\bar{t}$, with a $t\bar{t}$ pair. Four-top final states are particularly relevant in searches for heavy scalars and pseudoscalars, as the signal-background interference is negligible for associated production with $t\bar{t}$ compared to loop-induced production from gg initial states (Section 3.2.2). It should be noted, though, that the production cross-section for associated production is significantly lower than for loop-induced production.

Four-top final states are characterized by a high object multiplicity. Orthogonal signal regions can be defined based on the multiplicity of leptons (e, μ) in the final state, which corresponds to the number of top quarks with a leptonically decaying W boson.

The ATLAS Collaboration recently found evidence (4.3σ observed, 2.4σ expected significance) for four-top-quark production in a search focusing on the multilepton final state conducted on 139 fb^{-1} of $\sqrt{s} = 13 \text{ TeV}$ pp collision data [73]. The result is consistent with the SM prediction for four-top production within 1.7σ . A subsequent dedicated search for BSM four-top production on the same dataset specifically targets $t\bar{t}$ -associated production of heavy scalar or pseudoscalar Higgs bosons A/H decaying to $t\bar{t}$ ($t\bar{t} A/H \rightarrow t\bar{t}t\bar{t}$) [74]. It is based on and extends the analysis strategy of Ref. [73] to increase the sensitivity to A/H production. In both the SM and BSM searches, events are required to contain either a same-sign lepton pair or at least three leptons. A multivariate discriminant based on a boosted decision tree (BDT) is used to separate between SM four-top production and other background processes, using event-level information such as jet and b -jet multiplicity as well as additional kinematic variables. The BSM search relies on a second BDT to subsequently distinguish between BSM and SM four-top production. This second BDT is parameterized as a function of the mass of the heavy Higgs boson by introducing the mass as a labeled input in the training [75]. The main, irreducible backgrounds arise from associated production of a $t\bar{t}$ pair with a boson and additional jets ($t\bar{t} + W + \text{jets}$, $t\bar{t} + Z + \text{jets}$, $t\bar{t} + h + \text{jets}$). They are estimated using MC simulations with additional data-driven corrections applied in the case of $t\bar{t} + W + \text{jets}$ production. Smaller, reducible backgrounds arise mostly from $t\bar{t} + \text{jets}$ and $tW + \text{jets}$ production with misidentified charge or fake/nonprompt leptons. These smaller backgrounds are estimated from data using dedicated control regions. No significant excess of events over the SM prediction is observed in the BSM four-top search and the results are interpreted in the context of a type-II 2HDM. No dedicated interpretation in the context of DM models has been performed. The constraints on the type-II 2HDM with $m_A = m_H$, however, indicate that this search can improve upon the current four-top constraints on the 2HDM + a parameter space included in the latest 2HDM + a summary plots of Ref. [76] (Section 4.3.1), which are based on a search in the single-lepton channel using 36 fb^{-1} of $\sqrt{s} = 13 \text{ TeV}$ data [77].

The CMS Collaboration reported an observed (expected) significance for $t\bar{t}\bar{t}\bar{t}$ of 2.6σ (2.7σ) in the multilepton channel using 137 fb^{-1} of $\sqrt{s} = 13 \text{ TeV}$ pp collision data [78]. The search relies on a new multivariate classifier to maximize the sensitivity to the SM $t\bar{t}\bar{t}\bar{t}$ signal. As in the equivalent ATLAS search, the main backgrounds from $t\bar{t} + \text{boson} + \text{jets}$ production are estimated using MC simulations. Data-driven corrections are applied in the cases of $t\bar{t} + W + \text{jets}$ and $t\bar{t} + Z + \text{jets}$ production. Backgrounds arising from charge misidentification or fake/nonprompt leptons are estimated from data. This result has been used to constrain scalar and pseudoscalar production in 2HDMs as well as in the simplified DM model with a scalar or pseudoscalar mediator (Section 2.2.1). No dedicated interpretation for the 2HDM + a is available, although the constraints on type-II 2HDMs suggest that the search will also constrain the 2HDM + a parameter space.

The searches described above have been optimized for nonresonant $t\bar{t}\bar{t}\bar{t}$ production and/or production of heavy scalar or pseudoscalar resonances, including resonance masses below 1 TeV. An additional search targeting top-philic vector and axial-vector (Z') resonances with masses $> 1 \text{ TeV}$ was conducted by the ATLAS Collaboration. The preliminary

result relies on 139 fb^{-1} of $\sqrt{s} = 13 \text{ TeV}$ data [79]. Unlike other searches in the $t\bar{t}\bar{t}$ final state, this search was designed to reconstruct the BSM resonance explicitly from a pair of reclustered jets identified as merged top quarks. The results can, in principle, be used to constrain purely top-philic vector or axial-vector mediators to which classic $t\bar{t}$ resonance searches, which assume Z' production from light-quark or gluon initial states (Section 3.2.2), may not be sensitive. A dedicated interpretation of this search in the context of DM models is left to future work.

3.2.4. $tbH^\pm(tb)$

Final states with two top and two bottom quarks are sensitive to the associated production of a charged Higgs boson H^\pm with a top and a bottom quark (tb) and its subsequent decay to tb .

The ATLAS Collaboration published a search for $tbH^\pm(tb)$ production using 139 fb^{-1} of $\sqrt{s} = 13 \text{ TeV}$ data [80]. It targets charged Higgs boson masses in the range 0.2–2.0 TeV. Events are required to contain exactly one electron or muon to suppress the large backgrounds from strong multi(b)-jet production. The selected events are further classified according to the number of reconstructed jets and the number of b -jets among them. A neural network is used to enhance the separation between signal and background. The dominant background for this search is composed of $t\bar{t}$ jets events as well as single-top production in the Wt channel [81]. The backgrounds are modeled using MC simulations with additional data-driven corrections derived in a dedicated control region.

A search for charged Higgs bosons decaying into a top and a bottom quark in the 0-lepton final state was performed by the CMS Collaboration using proton–proton collision at $\sqrt{s} = 13 \text{ TeV}$ from 2016 [82]. Two different scenarios were studied: the associated production with a top and bottom quark and the s -channel production of a charged Higgs. The results were combined with a search in final states with one or two leptons [83]. For production in association with a top quark, upper limits at the 95% confidence level on the charged Higgs production cross-section and branching fraction of 9.25 to 0.005 pb were obtained for charged Higgs masses in the range of 0.2 to 3 TeV. While there is no DM interpretation of the result by the CMS Collaboration, the result from ATLAS was interpreted in a 2HDM + a scenario, as further detailed in Section 4.3.1.

4. Results

4.1. Vector and Axial-Vector Mediators

4.1.1. Flavor-Conserving Interaction

Strong constraints on visible decays of the axial-vector (Figure 7) or vector (Figure 8) mediator $m_{Z'}$ are obtained from a variety of resonance and related searches that probe mediator masses in the range between 50 GeV [84] and 5000 GeV [76].

The latest constraints on axial-vector mediators released by the ATLAS Collaboration and based on data from pp collisions at $\sqrt{s} = 13 \text{ TeV}$ are shown in Figure 7. The coupling of the mediator to leptons is set to zero ($g_\ell = 0$), while the coupling to DM is set to unity ($g_\chi = 1.0$) and the DM mass is taken to be 10 TeV to kinematically suppress invisible mediator decays and highlight the interplay of constraints on visible mediator decays.

In the high mediator mass range, the main sensitivity comes from two searches for di-jet resonances, referred to as *di-jet* and *di-jet angular*. The former aims to identify local resonant enhancements in the di-jet invariant mass spectrum and targets narrow mediator widths. The latter, for which no results on the full LHC Run 2 dataset are available, relies on the di-jet angular separation to identify broader mediator widths that cannot be probed by the search in the invariant mass spectrum. Neither of the searches imposes quark-flavor specific selection requirements, and hence are sensitive to all possible hadronic decays of the mediator.

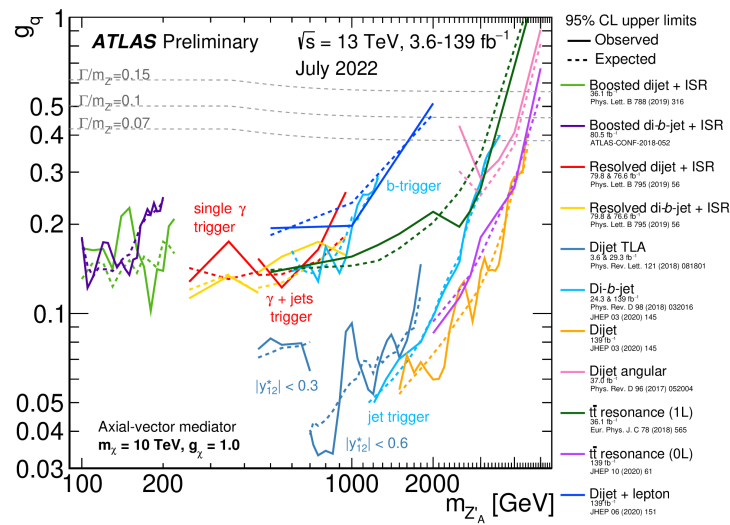


Figure 7. Upper limits at 95% CL on the coupling g_q of the mediator to quarks in a simplified model with a vector or axial-vector mediator obtained from different types of resonance searches using data from pp collisions at $\sqrt{s} = 13$ TeV. The DM mass is $m_\chi = 10$ TeV and its coupling to the mediator is $g_\chi = 1$ [76].

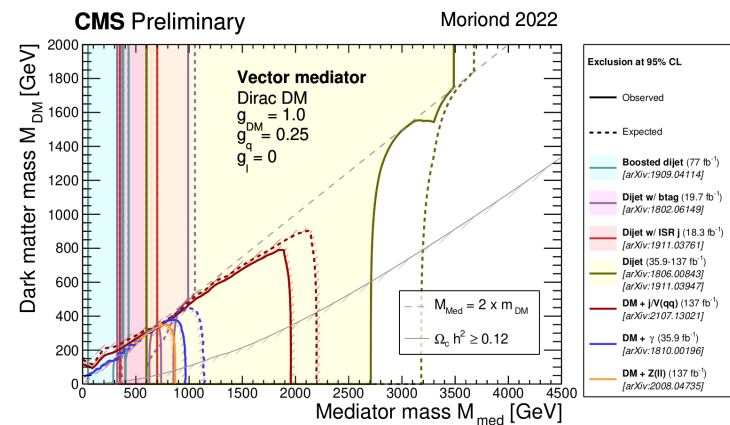


Figure 8. 95% CL observed and expected exclusion regions on vector mediators in the DM–mediator mass plane from searches with visible and invisible final states released by the CMS Collaboration [84]. Exclusions are computed for a leptophobic scenario with $g_l = 0$, a universal quark coupling of $g_q = 0.25$, and a DM coupling of $g_{DM} = 1.0$.

Searches for $t\bar{t}$ resonances, which rely on top-quark identification algorithms to specifically identify the decays of the mediator to top quarks, have a slightly lower expected sensitivity to the coupling g_q than di-jet searches, although the observed limit is stronger than that from the di-jet search in some small regions of the mediator mass where the di-jet observed limit fluctuates upward. The use of top-quark identification allows for a stronger suppression of SM backgrounds compared to di-jet and also di- b -jet searches, in particular the background from strong multijet production. This effect partially compensates the disadvantage of probing only roughly $\frac{1}{6}$ of the hadronic mediator decays.

In Figure 8, constraints on vector mediators in the plane of the DM and the mediator mass from the CMS Collaboration [84] are shown. Different from Figure 7, results from visible and invisible decays are summarized. While searches with invisible final states are only possible when the mediator mass is about twice the DM mass, the sensitivity of searches for visible decays only depends on the DM mass through the width of the mediator. When the decay channel to DM particles opens up, the width of the mediator increases and resonant searches become less sensitive. The best sensitivity to vector mediators from $p\bar{p}$ searches is provided by DM searches with initial state radiation either from a gluon/quark

jet or from the hadronic decay of a vector boson [85]. Searches with visible final states achieve best sensitivity down to 50 GeV when looking for a large radius jet that recoils against the mediator [86]. At high mass, the strongest constraints are obtained from di-jet searches [87]. The searches discussed in Section 3.2.2 probing vector mediators decaying into $t\bar{t}$ are not shown, as no dedicated interpretation of these results were performed in models of DM by the CMS Collaboration. However, the interpretation of the searches in generic vector particle models show comparable sensitivity between the results released by the ATLAS and CMS collaborations.

The collider constraints on simplified models with a vector or axial-vector mediator can be translated into limits on the spin-dependent DM–proton or DM–neutron and spin-independent DM–nucleon scattering cross-sections as a function of the DM mass to allow for a comparison with results from direct-detection experiments [88]. It should be noted that such a sensitivity comparison is highly dependent on the choice of model parameters, such as the mediator coupling type, as illustrated in the following. In Figure 9, constraints on the spin-independent DM–nucleon scattering cross-section (left) and the spin-dependent DM–neutron scattering cross-section (right) are shown for the case of a vector mediator and an axial-vector mediator, respectively. In the former case, the sensitivity from direct-detection experiments supersedes that from collider searches by several orders of magnitude for DM masses above 10 GeV. For smaller DM masses, collider experiments dominate the sensitivity as the sensitivity of direct-detection experiments is limited by the very low energy recoils that such low-mass DM particles would induce. In the case of an axial-vector mediator, collider experiments dominate the sensitivity across the studied DM mass range. A detailed discussion of the interplay between collider and direct-detection experiments in simplified models with a vector or axial-vector mediator can be found in Ref. [19].

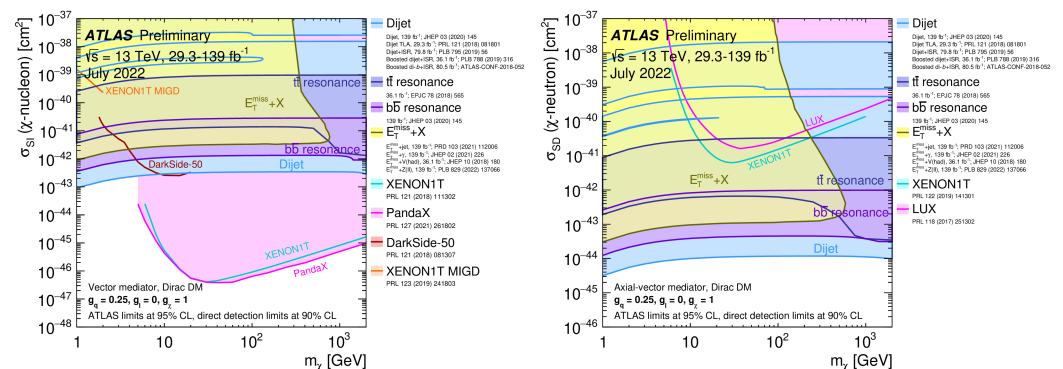


Figure 9. Upper limits on the spin-independent DM–nucleon scattering cross-section (left) and spin-dependent limits on the DM–neutron scattering cross-section (right) as a function of the DM mass, obtained from searches with the ATLAS detector as well as relevant direct-detection experiments, are summarized [76]. The limits for the spin-independent (spin-dependent) case are derived for the hypothesis of a leptophobic ($g_l = 0$) vector (axial-vector) mediator with a universal quark coupling of $g_q = 0.25$ and a DM coupling of $g_{DM} = 1.0$. The ATLAS limits are at 95% CL while the direct-detection results are at 90% CL.

4.1.2. Flavor-Changing Interaction

The strongest constraints on the VFC model are obtained from searches targeting same-sign tt and $p_T^{\text{miss}} + t$ production on 36 fb^{-1} of pp collision data [19]. Results for two representative parameter planes are shown in Figure 10.

The left plot of Figure 10 shows a scan in the mediator mass versus the flavor-changing coupling g_{ut} while fixing the remaining two parameters at $m_\chi = 1 \text{ GeV}$ and $g_\chi = 1$. The $p_T^{\text{miss}} + t$ search provides stronger constraints on g_{ut} at lower mediator masses, excluding g_{ut} down to 0.07 at 1 TeV, while the same-sign tt search is more sensitive for mediator masses $> 1.6 \text{ TeV}$, still excluding $g_{ut} > 0.3$ at 3 TeV. Mediator masses below 1 TeV were probed by the CMS Collaboration at $\sqrt{s} = 13 \text{ TeV}$ and are shown in Figure 11. The $p_T^{\text{miss}} + t$

search discussed in Section 3.1.1 is able to exclude couplings as low as 0.03 for mediator masses of 200 GeV.

The right plot of Figure 10 shows a scan in the invisible branching ratio of the mediator $\mathcal{BR}(\chi\chi)$ and the coupling g_{ut} . The constraints derived from the same-sign $t\bar{t}$ search exhibit only a weak dependence on $\mathcal{BR}(\chi\chi)$ due to the fact that the sensitivity of this process is dominated by the t -channel exchange of the mediator (middle and right diagrams in Figure 2). This process is only indirectly sensitive to g_χ through the total width of the mediator in the t -channel exchange. The same-sign $t\bar{t}$ analysis, hence, dominates the sensitivity at low values of g_χ (and, hence, low values of $\mathcal{BR}(\chi\chi)$), while the $p_T^{\text{miss}} + t$ analysis dominates the sensitivity at large values of $\mathcal{BR}(\chi\chi)$, excluding g_{ut} down to almost 0.06 at $\mathcal{BR}(\chi\chi) = 1$.

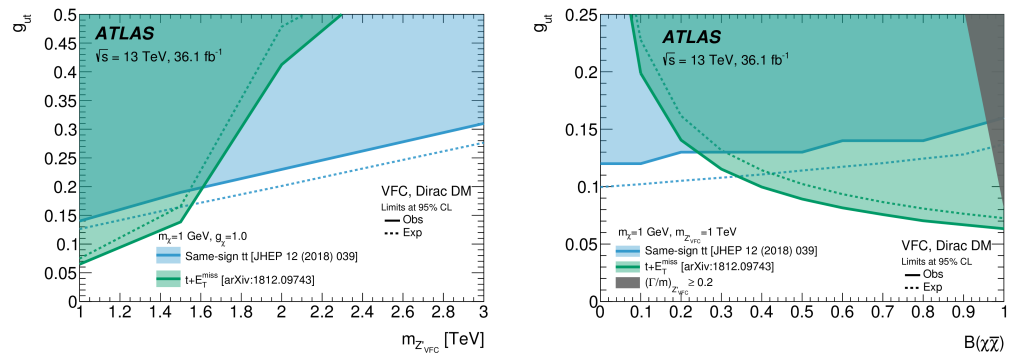


Figure 10. Regions in the $(m_{Z'_{VFC}}, g_{ut})$ (left) and the $(\mathcal{BR}(\chi\chi), g_{ut})$ plane (right) of the VFC model excluded at 95% CL by searches in the same-sign $t\bar{t}$ and $p_T^{\text{miss}} + t$ final states [19].

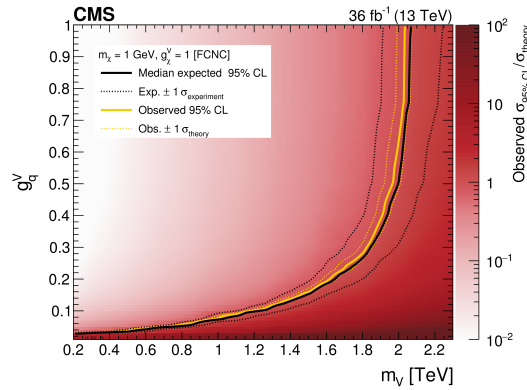


Figure 11. Exclusion limits for the VFC model in the two-dimensional plane spanned by the mediator mass and the coupling between the mediator and quarks released by the CMS Collaboration [44]. The observed exclusion range is shown as a yellow solid line, while the yellow dashed lines show the cases in which the predicted cross-section is shifted by the assigned theoretical uncertainty. The expected exclusion range is indicated by a black solid line, and the experimental uncertainties are shown in black dashed lines.

4.2. Scalar and Pseudoscalar Mediators

4.2.1. Color-Neutral Interaction

Simplified models with a color-neutral scalar or pseudoscalar mediator were constrained by searches targeting invisible mediator decays at the ATLAS and CMS experiments using data from pp collisions at $\sqrt{s} = 13$ TeV. The most recent constraints from the CMS Collaboration based on $p_T^{\text{miss}} + t\bar{t}$ events are shown in Figure 12, while Figure 13 shows the most recent summary from the ATLAS Collaboration.

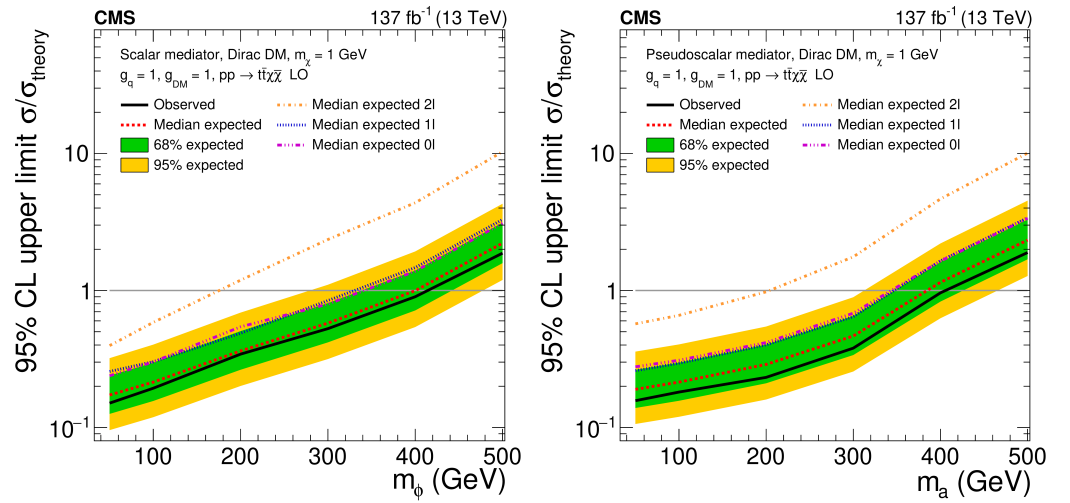


Figure 12. Expected (dashed line) and observed (solid line) upper limits at the 95% CL on the ratio of the excluded and predicted cross-section at leading-order for a DM particle with a mass of 1 GeV as a function of the mediator mass for a scalar (**left**) and pseudoscalar (**right**) mediator [57]. The green and yellow bands represent the regions containing 68 and 95%, respectively, of the distribution of limits expected under the background-only hypothesis. The mediator couplings are set to 1.

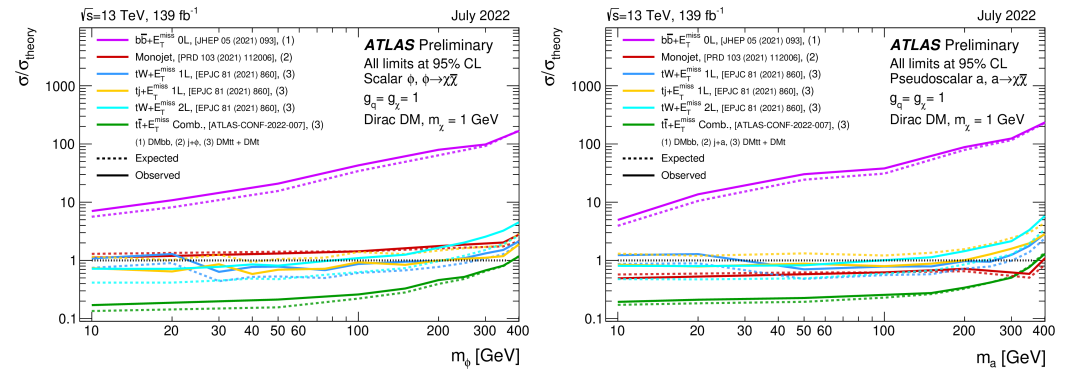


Figure 13. Upper limits at 95% CL on the production of a scalar ϕ (**left**) and pseudoscalar a (**right**) mediator as a function of the mediator mass [76]. The limits are expressed in terms of the ratio of the excluded cross-section and the cross-section calculated for a coupling assumption of $g = g_q = g_\chi = 1.0$. The latter was calculated at NLO for the $p_T^{\text{miss}} + t\bar{t}$ signatures and at LO for the $p_T^{\text{miss}} + tW/tj$ and $p_T^{\text{miss}} + j$ signatures.

Up to now, only $t\bar{t}$ -associated DM production has been probed by the CMS Collaboration using the full Run II dataset of 137 fb^{-1} [57]. The interpretation of this analysis in simplified models of scalar and pseudoscalar mediators is shown in Figure 12. Assuming a mediator coupling of 1 to DM and SM particles, masses up to 400 GeV and 420 GeV can be excluded for scalar and pseudoscalar mediators, respectively. While the sensitivities of the 0- and 1-lepton channels are comparable, the sensitivity of the 2-lepton channel is significantly weaker. The sensitivity of this channel can be further enhanced by exploring information sensitive to the spin of the mediator, which was not performed here. The exclusion limits for pseudoscalar mediators can be further extended up to 470 GeV by $p_T^{\text{miss}} + \text{jet}$ searches [85].

The results shown in Figure 13 are obtained from analyses targeting $p_T^{\text{miss}} + t\bar{t}$, $p_T^{\text{miss}} + tW$, $p_T^{\text{miss}} + tj$, $p_T^{\text{miss}} + b\bar{b}$, and $p_T^{\text{miss}} + \text{jet}$ production using the full ATLAS Run 2 dataset of 139 fb^{-1} [76]. The sensitivity across most of the mediator mass region is dominated by a statistical combination of three searches for $p_T^{\text{miss}} + t\bar{t}$ production in the 0-, 1-, and 2-lepton channels (Section 3.1.3). In the scenario with a scalar mediator, the statistical combination of the $p_T^{\text{miss}} + t\bar{t}$ searches provides the strongest constraints across

the probed mediator mass range, while for the pseudoscalar case, the dominant constraints for $m_{\phi/a} > 300$ GeV are obtained from $p_T^{\text{miss}} + \text{jet}$ searches. Searches targeting the $p_T^{\text{miss}} + b\bar{b}$ signature provide significantly weaker constraints on this model. However, as explained in Section 2.2.1, in UV completions of the simplified model, the couplings to up-type quarks can be suppressed compared to those to down-type quarks, making $p_T^{\text{miss}} + b\bar{b}$ searches a relevant complement to $p_T^{\text{miss}} + t\bar{t}$ searches. Searches targeting DM production with a single top quark ($p_T^{\text{miss}} + t\bar{t}$ and $p_T^{\text{miss}} + tW$; see Section 2.2.1) have a similar sensitivity to the individual searches for $p_T^{\text{miss}} + t\bar{t}$ production. They were not included in the statistical combination as they are not orthogonal to the searches in the $p_T^{\text{miss}} + t\bar{t}$ final states by construction.

If $m_{\phi/a} > 2 \cdot m_t$, searches targeting visible mediator decays to top quarks are also sensitive to the production of scalar or pseudoscalar mediators. Two different modes can contribute: gluon-induced mediator production and production of a mediator in association with $t\bar{t}$. Searches targeting both modes were performed, as discussed in Sections 3.2.2 and 3.2.3, respectively. However, only the results of a search for four-top production conducted by the CMS Collaboration were interpreted in the context of simplified models with a scalar or pseudoscalar mediator. The results are shown in Figure 14 as upper limits on the cross-section of associated production of the mediator with top quarks times the branching ratio of the mediator decay to $t\bar{t}$. Masses between 350 GeV and 450 (510) GeV for a scalar (pseudoscalar) mediator are excluded.

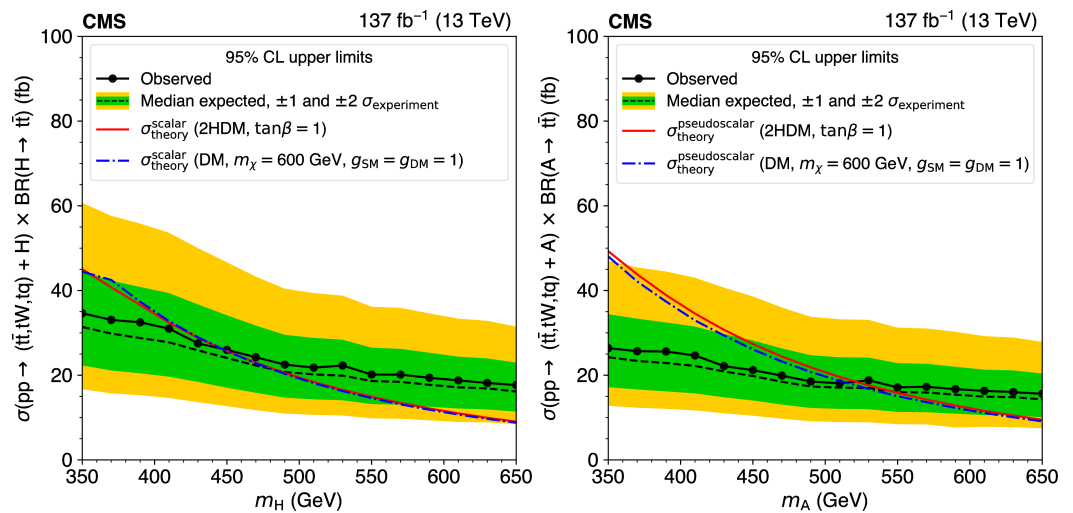


Figure 14. Upper limits at 95% CL on the production of a scalar ((left), called H here instead of ϕ) and pseudoscalar ((right), called A here instead of a) mediator as a function of the mediator mass [76]. The limits are expressed in terms of an upper limit on the production cross-section times the branching ratio of the mediator to $t\bar{t}$ and compared to the cross-section calculated at LO for a coupling assumption of $g = g_q = g_\chi = 1.0$ (here denoted as $g_{SM} = g_{DM} = 1.0$).

It should be noted that the reinterpretation of the results from searches targeting gluon-induced mediator production is significantly more involved than for the case of associated production due to the presence of strong signal-background interference (Section 3.2.2). The resulting interference patterns are highly model-dependent which means that a reinterpretation in the context of a different model requires the generation of the model-specific interference pattern and a subsequent rerunning of the full profile likelihood fit for these model-specific interference patterns.

4.2.2. Color-Charged Interaction

Models in which the color-charged mediator decays to a top quark and a DM particle are constrained by the searches in $p_T^{\text{miss}} + t$ final states discussed in Section 3.1.1. Mediator

masses up to 5 TeV can be excluded by the ATLAS Collaboration for coupling strength values $\lambda_t = 0.4$ and $g_{ds} = 0.6$, assuming a DM mass $m_\chi = 10$ GeV [43].

Results with a mixed scalar and pseudoscalar coupling to both SM quarks, as well as DM and top quarks, are provided by CMS Collaboration [44]. Assuming a coupling of 0.1 to SM quarks and of 0.2 to DM and top quarks, mediators with masses up to 3.3 TeV can be excluded for a dark matter mass of 100 GeV.

4.3. Extended Higgs Sectors

4.3.1. 2HDM with a Pseudoscalar Mediator

Constraints on the 2HDM + a are derived from a variety of searches targeting different production and decay modes of the mediator and the additional Higgs bosons. The most comprehensive summary of constraints was released by the ATLAS Collaboration [76]. These summary plots are based on results obtained on the partial or full Run 2 datasets. Not all of the latest searches on the full Run 2 dataset were reinterpreted in the context of the 2HDM + a . Updated summary plots will be released in the near future.

The constraints are evaluated as a function of the free parameters of the model described in Section 2.3. Two representative parameter scans in the (m_a, m_A) and the $(m_a, \tan \beta)$ plane highlighting the interplay of signatures involving top quarks with other types of signatures are shown in Figure 15. The constraints for other benchmark scans can be found in Ref. [76].

The sensitivity in the (m_a, m_A) plane for $\tan \beta = 1$, $\sin \theta = 0.35$, and $m_A = m_H = m_{H^\pm}$ is largely dominated by searches targeting the production of an invisibly decaying mediator with a Higgs or Z boson, leading to $p_T^{\text{miss}} + h$ and $p_T^{\text{miss}} + Z$ signatures, directly. These processes are dominated by diagrams involving the resonant production of a neutral Higgs bosons H or A that decays to ah or aZ , respectively. The sensitivity from searches for $p_T^{\text{miss}} + tW$ production, which can also proceed resonantly via a charged Higgs boson (Section 2.3), is subdominant in this parameter region.

Constraints that are largely complementary to those from $p_T^{\text{miss}} + X$ searches are obtained from a search targeting resonant-associated production of a charged Higgs boson H^\pm with a top–bottom-quark pair (tbH^\pm) with subsequent decay to a top–bottom-quark pair tb . These constraints exhibit only a weak dependence on the mediator mass m_a as this signature does not involve production of a mediator at leading order, and is, hence, only indirectly dependent on the mediator mass via its effect on the branching ratio to tb compared to those for other decays, such as $H^\pm \rightarrow aW^\pm, AW^\pm, HW^\pm$.

Searches targeting resonant production of the neutral Higgs bosons A/H , either via gluon fusion or $t\bar{t}$ -associated production, and their decay to $t\bar{t}$, leading to $t\bar{t}$ and $t\bar{t}\bar{t}$ final states, respectively, are expected to also provide complementary constraints to those from $p_T^{\text{miss}} + X$ searches in this parameter region, given that the choice $\tan \beta = 1$ favors the coupling of those Higgs bosons to top quarks. No constraints from $A/H(t\bar{t})$ have been derived for the 2HDM + a yet due to the presence of strong, model-dependent interference effects that make a straightforward reinterpretation of these searches in the context of other benchmark models difficult, as explained in Section 4.2.1. A search targeting $t\bar{t}A/H(t\bar{t})$ production was used to constrain the 2HDM + a parameter space (see below). It is based on 36 fb^{-1} of LHC Run 2 data and not sensitive at $\tan \beta = 1$, as shown in Figure 15 (right plot). The results of a search for $t\bar{t}A/H(t\bar{t})$ production in multilepton final states using 139 fb^{-1} of LHC Run 2 data indicate that A/H masses up to 700 GeV could be excluded in the 2HDM + a for the parameter region with $\tan \beta$ under consideration here [74].

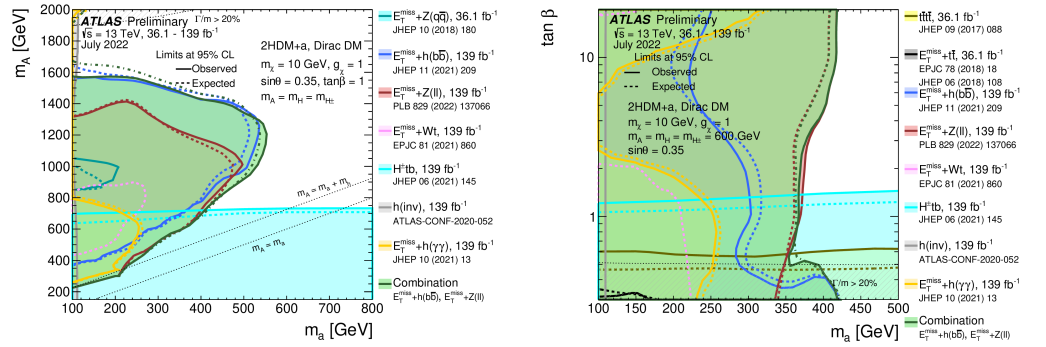


Figure 15. Regions in the 2HDM + a parameter space excluded at 95% CL by several individual searches targeting different signatures and a statistical combination of $p_T^{\text{miss}} + Z(\ell\ell)$ and $p_T^{\text{miss}} + h(b\bar{b})$ searches. The results are shown in the (m_a, m_A) plane (left) and the $(m_a, \tan\beta)$ plane (right). In the former case, $\tan\beta = 1$, while in the latter case, $m_A = 600$ GeV. In both cases, the conditions $\sin\theta = 0.35$ and $m_A = m_H = m_{H^\pm}$ are imposed. All results are based on either the full 139 fb^{-1} of pp collision data at $\sqrt{s} = 13$ TeV or a subset of that dataset amounting to 36 fb^{-1} [76].

In the $(m_a, \tan\beta)$ plane with $m_A = m_H = m_{H^\pm} = 600$ GeV (right plot in Figure 15), the sensitivity is again dominated by the statistical combination of the $p_T^{\text{miss}} + h(b\bar{b})$ and $p_T^{\text{miss}} + Z(\ell\ell)$ searches and the search for tbH^\pm (tb) production, which provide complementary constraints in this region of parameter space. Low values of $\tan\beta$ are fully excluded by the search for charged Higgs bosons decaying to tb . The constraints from the search targeting $t\bar{t}f\bar{f}$ production on 36 fb^{-1} of LHC Run 2 data are also shown. While they are notably weaker than the constraints from the charged-Higgs-boson search, which relies on the full Run 2 dataset amounting to 139 fb^{-1} , the results from the search for $t\bar{t}A/H(t\bar{t})$ on 139 fb^{-1} of LHC Run 2 data [74] (Section 3.2.3) indicate that this final state may provide a comparable exclusion power to the charged-Higgs-boson search if reinterpreted in the context of this model.

Searches for $p_T^{\text{miss}} + t\bar{t}$ production, which dominate the sensitivity to the simplified model with a color-neutral scalar or pseudoscalar mediator (Section 4.2.1), only weakly constrain the benchmark scenarios [38,39] probed at the LHC. It should, however, be noted that the $p_T^{\text{miss}} + t\bar{t}$ constraints shown in Figure 15 are based on only 36 fb^{-1} of LHC Run 2 data and the sensitivity is mainly limited by low event rates. Hence, significantly stronger constraints are expected from a reinterpretation of searches using the full 139 fb^{-1} of LHC Run 2 data [67]. The sensitivity of the $p_T^{\text{miss}} + t\bar{t}$ final state is expected to become comparable to that of searches in the $p_T^{\text{miss}} + h$ and $p_T^{\text{miss}} + Z$ final states for an integrated luminosity of 300 fb^{-1} , expected to be available after the end of LHC Run 3 (2022–2025) [32]. In this context, it should be noted that the cross-section for $p_T^{\text{miss}} + t\bar{t}$ production is suppressed by $\sin^2\theta$, making this process more sensitive for large values of $\sin\theta$ [32]. Furthermore, for $m_a > 2 \cdot m_t$, visible mediator decays to $t\bar{t}$ are possible, reducing the invisible branching ratio $a \rightarrow \chi\chi$ and, hence, the sensitivity of the $p_T^{\text{miss}} + t\bar{t}$ searches [32].

4.4. Scalar DE EFT Model

Searches in the $p_T^{\text{miss}} + t\bar{t}$ final state were used to constrain the \mathcal{L}_1 operator in the EFT model of scalar DE (Section 2.4). Results from three independent analyses, each targeting a different $t\bar{t}$ decay mode (0-, 1-, 2-lepton channels), were used. No statistical combination was performed. Instead, the constraint from the analysis yielding the smallest CL_s value for a given signal hypothesis was reinterpreted in the EFT model of DE. The strongest constraints arise from searches in the 0- and 1-lepton channels, with both contributing roughly equally.

The constraints are derived as a function of the effective coupling g_* associated with the UV completion of the EFT model and the effective mass scale M_1 . It is assumed that the EFT is valid for momentum transfers $Q_{\text{tr}} < g_* M$ [19]. For events failing this requirement,

a conservative approach to correct the final limits based on the fraction of valid events, referred to as iterative rescaling [18], is applied.

The regions excluded at 95% CL are shown in Figure 16. Mass scales < 200 GeV are excluded for $g_* > \pi^2$. The sensitivity of the $p_T^{\text{miss}} + t\bar{t}$ signature to softer effective couplings g_* is limited by the EFT criterion as $t\bar{t}$ -pair production typically involves large momentum transfers.

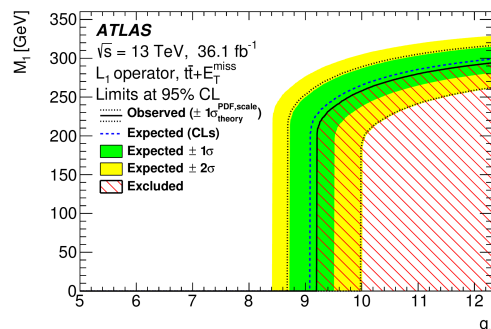


Figure 16. Regions in the plane of the effective coupling g_* associated with the UV completion of the EFT model and the effective mass scale M_1 for the \mathcal{L}_∞ operator excluded at 95% CL by searches in the $p_T^{\text{miss}} + t\bar{t}$ final state [19].

5. Discussion

A variety of searches targeting top-quark production in association with DM or via visible decays of mediator particles were conducted by the ATLAS and CMS collaborations. No significant deviation from the SM prediction was observed; therefore, the results were used to constrain DM in a variety of simplified models as well as scalar DE described in an EFT model. Signatures involving top quarks often provide sensitivity in parameter regions not covered by other DM searches, underlining their importance as sensitive probes of DM at colliders. They provide a particularly relevant probe of models involving new particles with Yukawa-like interactions, which imply preferred couplings to top quarks.

It should be noted that many of the results and summary plots presented in this review are preliminary, as various searches on the full LHC Run 2 collision data are still ongoing. Furthermore, not all of the existing results have been interpreted in relevant benchmark models. Further results of DM searches with top quarks are expected to be released by both collaborations in the near future.

6. Outlook

6.1. LHC Run 3

The nonobservation of WIMP DM at the LHC and various direct-detection experiments to date has prompted the particle physics community to place a stronger focus on models and searches for non-WIMP DM as well as uncovered DM signatures at the LHC that can be probed during LHC Run 3 (2022–2025) and/or via reinterpretations of existing searches on LHC Run 2 data [89–91]. A few notable examples involving signatures with top quarks are given in the following.

6.1.1. ALPs

Axions and axion-like particles (ALPs) [92,93] have received increasing attention in recent years. A novel strategy to search for ALPs and, more generally, pseudo-Nambu–Goldstone bosons (pNGB) at the LHC was proposed in Ref. [94], focusing on nonresonant searches that would be sensitive to ALPs produced as off-shell s -channel mediators. It is motivated by the fact that the pNGB nature of the ALPs implies that their couplings to the SM are dominantly derivative, which leads to a cross-section enhancement for nonresonant ALPs production at center-of-mass energies $\hat{s} \gg m_a$, where m_a denotes the mass of the ALP. The focus of recent studies is on constraining the ALP-boson (W, Z, h ,

g, γ) coupling via nonresonant $ZZ, \gamma\gamma,$ and gg [94], nonresonant ZZ and Zh [95], and nonresonant $WW, Z\gamma$ [96] production. The ALPs–fermion coupling can be predominantly probed via nonresonant $t\bar{t}$ production (illustrated by the left diagram in Figure 17) due to the Yukawa-like structure of the ALP–fermion couplings. No public results exist to date, but studies are ongoing.

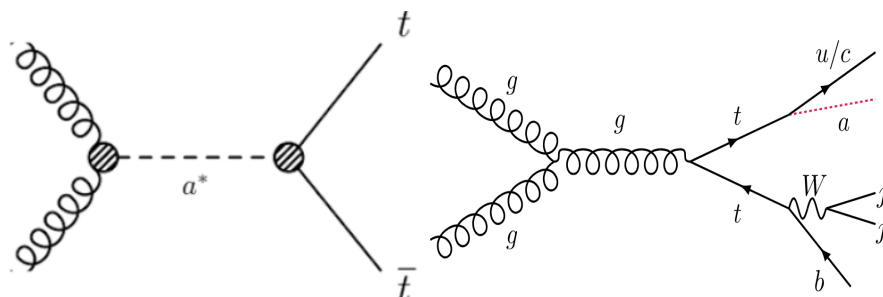


Figure 17. Schematic representation of nonresonant $t\bar{t}$ production via an off-shell s -channel ALP ((left), [97]) and SM $t\bar{t}$ production with subsequent decay of one of the top quarks to an up-type quark and a long-lived ALP ((right), [98]).

The ALPs–fermion coupling can also be probed in $p_T^{\text{miss}} + t\bar{t}$ final states. These are sensitive to $t\bar{t}$ -associated production of a single ALP with couplings to quarks derived from couplings to the bosonic sector and proportional to the fermion mass [99]. It should be noted that the p_T^{miss} distribution predicted for this signal process is softer on average than that predicted by, e.g., stop production in supersymmetric models, emphasizing the importance of keeping the p_T^{miss} threshold low in future searches.

Novel detector signatures involving exotic top-quark decays are predicted in models with flavor-violating ALPs [98], which are motivated by t -channel dark sector models [100] or Froggatt–Nielsen models of flavor [101]. These models predict flavor-violating decays of the top quark to an up-type quark and an ALP, with the ALP decaying predominantly to hadrons, either promptly or with a long lifetime. Precision measurements of single-top-quark production can constrain the parameter space of such models for prompt ALPs decays to jets and detector-stable ALPs. Displaced detector signatures are predicted for nonprompt ALPs decays within the detector volume. A novel search was proposed [98], focusing on exotic top-quark decays from SM $t\bar{t}$ production (right diagram in Figure 17), where one of the top quarks decays into an up-type quark and an ALP, which in turn decays into a displaced narrow jet within the calorimeter volume. This and other signatures involving long-lived particles (LLP) in top-quark decays have not yet been probed in dedicated searches at the LHC. They remain an exciting prospect for the analysis of LHC Run 3 data within the currently fast-growing field of LLPs searches at the LHC, a field that benefits in particular from novel trigger and reconstruction algorithms deployed by the ATLAS and CMS experiments for Run 3 data-taking.

6.1.2. Composite Pseudo-Nambu–Goldstone Bosons

Signatures with top quarks can also be used to probe still-viable WIMP models in which WIMP DM is made up of composite pNGBs [102]. In these models, both the SM Higgs boson and DM emerge from a TeV-scale strongly-coupled sector as pNGBs, and the SM–DM interaction is provided by higher-dimensional derivative couplings with the Higgs fields, which leads to a strong suppression of the DM scattering rates against SM particles. Thus, these models evade the strong constraints from direct-detection experiments, making collider searches particularly relevant. The pNGB DM contains additional interactions with the SM sector, besides the derivative Higgs portal, with preferential couplings to third-generation fermions being well motivated [102]. If couplings to top quarks are preferred over couplings to bottom quarks, e.g., in the case of Yukawa-type couplings, pNGB models can be probed at the LHC via associated production of pNGB DM with $t\bar{t}$ or a single top quark, i.e., in $p_T^{\text{miss}} + t\bar{t}$ or $p_T^{\text{miss}} + t + X$ final states. Two possible production modes of

pNGB leading to $p_T^{\text{miss}} + tW$ final states via the Higgs portal and direct DM–top interactions are shown in Figure 18. Searches in these final states are complementary to searches for invisible Higgs boson decays in vector boson fusion (VBF) production as they are sensitive to pNGB interactions with fermions not accessible via the latter. Reinterpretations of existing $p_T^{\text{miss}} + t\bar{t}$ and $p_T^{\text{miss}} + tW$ searches, as well as possible optimizations of future searches for pNGB production, could be interesting to explore during LHC Run 3.

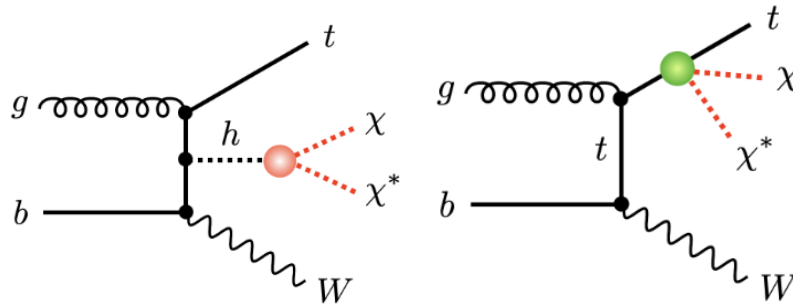


Figure 18. Schematic representation of $p_T^{\text{miss}} + tW$ production via DM–Higgs operators (left) and DM–top operators in an EFT of composite pNGBs [102].

6.1.3. Dark Mesons

Final states with multiple top quarks are predicted in models with a strongly coupled dark sector consisting of composite particles that carry electroweak, but no color, charges [103]. These models not only address the hierarchy problem but can also provide a DM candidate in the form of a composite meson whose decays are suppressed via an automatic accidental symmetry.

The most promising target for collider searches is the dark meson sector, consisting of dark vector mesons ρ_D and dark pions π_D [103]. Signatures with multiple top or bottom quarks are predicted if a pair of dark pions with gaugephobic couplings to the SM is produced from the decay of a resonantly produced ρ_D ($pp \rightarrow \rho_D \rightarrow \pi_D \pi_D$). The dark pions then decay predominantly into third-generation fermions, with decays to $t\bar{t}$ (tb) dominating the branching fraction for π_D^0 (π_D^\pm) if the pion mass is above the $t\bar{t}$ (tb) production threshold. Depending on the charge of the intermediate ρ_D , different final states involving third-generation quarks are possible: $b\bar{b}t\bar{t}$, $t\bar{t}b\bar{b}$, $t\bar{t}t\bar{b}$.

Existing searches in multitop final states only weakly constrain the parameter space of these models [103]. This is due to the fact that small masses of the ρ_D and π_D are still viable, which means that the SM fermions in the final state tend to be rather soft. In searches at $\sqrt{s} = 13$ TeV, in particular, higher thresholds are imposed on the energy/momenta of the final-state objects or their vector sum. In order to probe dark pions, or more generically strongly-coupled-like models, dedicated searches targeting final states with a high multiplicity of low-momentum objects compatible with the decays of one or several low-momentum top quarks are needed.

6.2. HL-LHC and HE-LHC

The physics potential for DM searches involving top quarks during the high-luminosity phase of the LHC (HL-LHC, starting 2028) and the perspectives for a possible future high-energy LHC (HE-LHC) were studied in the context of a 2019 CERN Yellow Report [104]. The final HL-LHC dataset is expected to amount to an integrated luminosity of 3000 fb^{-1} at a center-of-mass energy $\sqrt{s} = 14$ TeV. The HE-LHC scenario relies on the assumption of a possible further upgrade of the LHC to a 27 TeV pp collider with a final integrated luminosity of $15,000 \text{ fb}^{-1}$.

Sensitivity studies were performed for the $p_T^{\text{miss}} + t\bar{t}$, $p_T^{\text{miss}} + tW$, $p_T^{\text{miss}} + t$, $t\bar{t}$, and $t\bar{t}t\bar{t}$ signatures within various benchmark models, including simplified models with a scalar or pseudoscalar mediator (Section 2.2.1), simplified models with a vector mediator with a flavor-changing coupling to the top and up-quark (Section 2.1.2), and the 2HDM + a

(Section 2.3). These studies were mostly based on the analysis tools and strategies used for the analysis of the partial LHC Run 2 dataset (2015–2016). They do not include further improvements, such as new machine-learning-based tools or background estimation strategies, implemented for the later analyses of the full LHC Run 2 dataset. A full review of the results of these sensitivity studies across the different final states and models is beyond the scope of this article, but a few general observations can be made. Overall, both the increase in integrated luminosity (HL-LHC) and center-of-mass energy (HE-LHC) lead to a significant sensitivity increase across the different final states. For example, the mass range for a (pseudo-)scalar mediator expected to be excluded by $p_T^{\text{miss}} + t\bar{t}$ searches in the simplified model of Section 2.2.1 with $g = g_q = g_\chi = 1.0$ (compare Figure 13) is expected to increase by a factor of two for the HL-LHC compared to the expected sensitivity for LHC Run 3, and by another factor of two for the HE-LHC compared to the HL-LHC.

The sensitivity of most of the searches is dominated by the systematic uncertainties on the main (often irreducible) background processes, for example, $t\bar{t} + V$ in the case of $p_T^{\text{miss}} + t\bar{t}$ searches. In $t\bar{t}$ final states, these typically arise from two sources: firstly, uncertainties related to reconstructed objects, such as the energy scale for hadronic jets, and, secondly, uncertainties arising from the modeling of SM processes, such as missing higher-order corrections. These uncertainties can vary between a few percent and a few tens of percent, depending on the process and kinematic region. The former are expected to decrease with increasing integrated luminosity as the statistical uncertainties on the measurements from which they are derived are reduced accordingly. A further reduction of these uncertainties can be expected due to the development of better and more refined calibration methods. The latter can be reduced significantly through profiling in a likelihood fit to data if appropriate, background-enriched control regions are defined. Improved theoretical predictions, for example, for differential cross-sections at higher orders in perturbation theory, can also significantly boost the sensitivity of many searches.

In the case of the HE-LHC, in addition to the improvements due to the larger integrated luminosity, the larger center-of-mass energy provides access to mediator masses beyond the kinematic reach of the (HL-)LHC and to processes with small signal cross-sections.

6.3. FCC-hh

Similar considerations to those for the HE-LHC apply to the case of a potential future hadron collider operating at center-of-mass energies beyond that of the LHC and HE-LHC. The most prominent example is that of the FCC-hh, the Future Circular Collider, in its operation mode as a hadron collider with a center-of-mass energy of $\sqrt{s} = 100$ TeV [105]. Few dedicated studies regarding the sensitivity of DM searches with top quarks at the FCC-hh exist. For example, in Ref. [106], the sensitivity of the 2-lepton $p_T^{\text{miss}} + t\bar{t}$ final state to Higgs portal models and their extensions is discussed. In general, a significant increase in the accessible mass range of both mediators and DM particles is expected, as well as a significant increase in the sensitivity to smaller DM–SM couplings, rendering detector signatures involving decays of long-lived particles away from the interaction point that is highly relevant. Moreover, top quarks appearing in the final states of FCC-hh collision can be extremely boosted, underlining the need for high-resolution detectors to identify very collimated decays, as well as the use of advanced pattern recognition methods for top-quark tagging. A particularly interesting observation is the fact that associated production of a single Higgs boson with $t\bar{t}$ becomes the dominant Higgs boson production mode at Higgs boson transverse momenta of 1–2 TeV and above, a kinematic regime that would be well-populated at the FCC-hh [107]. According to initial studies [107], searches for invisible Higgs boson decays in this production mode would feature a very low background contamination ($S/B \sim 1$) and, hence, provide excellent sensitivity to Higgs portal models with small couplings. The corresponding final state would be $p_T^{\text{miss}} + t\bar{t}$ with highly boosted top quarks.

6.4. Future e^+e^- Colliders

No studies of DM searches with top quarks exist for future e^+e^- colliders, such as the International Linear Collider (ILC) [108], the Compact Linear Collider (CLIC) [109,110], the Future Circular Collider FCC-ee [111,112], and the Circular Electron Positron Collider (CEPC) [113,114]. This can be mostly attributed to the fact that these machines are primarily designed for Higgs boson and top-quark precision measurements, rather than a broad range of BSM (including DM) searches, and that their foreseen center-of-mass energies are, in many cases, below or close to the $t\bar{t}$ production threshold. For example, operation modes at $\sqrt{s} = 240$ GeV (250 GeV), i.e., around the maximum of the Zh production cross-section, are foreseen for the FCC-ee and the CEPC (ILC). Additional operation modes in the range 350–365 GeV (FCC-ee, CEPC) and 380 GeV (CLIC) are foreseen for top-quark precision measurements. Higher center-of-mass energies of 1 TeV (ILC) and 1–3 TeV could be possible for the linear e^+e^- machines to allow for wider range of BSM searches. Hence, direct DM production in association with at least one top quark, leading to $p_T^{\text{miss}} + t\bar{t}$ and $p_T^{\text{miss}} + t + X$ final states, while in principle possible, is trivially limited by the available center-of-mass energy. Nevertheless, the foreseen precision scans of the $t\bar{t}$ production threshold at the FCC-ee could, in principle, be sensitive to anomalous resonant or nonresonant $t\bar{t}$ production linked with DM or DM mediators as well as anomalous top-quark decays. Further studies are needed to understand the prospects for DM searches with top quarks at future e^+e^- colliders.

6.5. Conclusions

Collider signatures with top quarks provide sensitive probes of DM predicted by a wide range of models, and possibly even to DE signatures. Searches targeting top-quark production in association with DM or via visible decays of mediator particles have been performed by the ATLAS and CMS Collaborations, with many searches on the full LHC Run 2 collision data still ongoing. As shown in this review, DM searches involving top quarks often provide sensitivity in parameter regions not covered by other DM searches, underlining their importance as sensitive probes of DM at colliders. The upcoming LHC Run 3 opens up further opportunities to improve upon existing results or to explore new signatures, for example, involving top quarks in association with long-lived particle signatures.

Author Contributions: All authors equally contributed to all the parts of the manuscript. All authors have read and agreed to the published version of the manuscript.

Funding: This review article was produced without external funding.

Data Availability Statement: Not applicable.

Acknowledgments: K.B. thanks the Helmholtz Association for the support through the “Young Investigator Group” initiative. The authors acknowledge funding by the Deutsche Forschungsgemeinschaft (DFG, German Research Foundation) under Germany’s Excellence Strategy—EXC 2121 “Quantum Universe”—390833306.

Conflicts of Interest: The authors declare no conflict of interest.

Abbreviations

The following abbreviations are used in this manuscript:

DM	Dark matter
DE	Dark energy
EFT	Effective field theory

References

1. Trimble, V. Existence and Nature of Dark Matter in the Universe. *Annu. Rev. Astron. Astrophys.* **1987**, *25*, 425. [CrossRef]
2. Bertone, G.; Hooper, D.; Silk, J. Particle dark matter: evidence, candidates and constraints. *Phys. Rep.* **2005**, *405*, 279. [CrossRef]

3. Feng, J.L. Dark Matter Candidates from Particle Physics and Methods of Detection. *Annu. Rev. Astron. Astrophys.* **2010**, *48*, 495. [[CrossRef](#)]
4. Hinshaw, G.; Larson, D.; Komatsu, E.; Spergel, D. N.; Bennett, C. L.; Dunkley, J. M.; Nolte, R.; Halpern, M.; Hill, R. S.; Odegard, N. Nine-Year Wilkinson Microwave Anisotropy Probe (WMAP) Observations: Cosmological Parameter Results. *Astrophys. J. Suppl.* **2013**, *208*, 19. [[CrossRef](#)]
5. Planck Collaboration. Planck 2018 results. I. Overview and the cosmological legacy of Planck. *Astron. Astrophys.* **2020**, *641*, A1. [[CrossRef](#)]
6. Steigman, G.; Turner, M.S. Cosmological constraints on the properties of weakly interacting massive particles. *Nucl. Phys. B* **1985**, *253*, 375. [[CrossRef](#)]
7. Evans, L.; Bryant, P. LHC Machine. *JINST* **2008**, *3*, S08001. [[CrossRef](#)]
8. Billard, J.; Boulay, M.; Cebrián, S.; Covi, L.; Fiorillo, G.; Green, A.; Kopp, J.; Majorovits, B.; Palladino, K.; Petricca, F. Direct detection of dark matter—APPEC committee report. *Rept. Prog. Phys.* **2022**, *85*, 056201. [[CrossRef](#)]
9. Heros, P.d.l. Status, Challenges and Directions in Indirect Dark Matter Searches. *Symmetry* **2020**, *12*, 1648. [[CrossRef](#)]
10. ATLAS Collaboration. The ATLAS Experiment at the CERN Large Hadron Collider. *JINST* **2008**, *3*, S08003.
11. CMS Collaboration. The CMS experiment at the CERN LHC. *JINST* **2008**, *3*, S08004.
12. Buchmueller, O.; Doglioni, C.; Wang, L.T. Search for dark matter at colliders. *Nat. Phys.* **2017**, *13*, 217–223. [[CrossRef](#)]
13. Boveia, A.; Doglioni, C. Dark Matter Searches at Colliders. *Ann. Rev. Nucl. Part. Sci.* **2018**, *68*, 429. [[CrossRef](#)]
14. CDF Collaboration. Observation of top quark production in ppbar collisions with the Collider-Detector at Fermilab. *Phys. Rev. Lett.* **1995**, *74*, 2626. [[CrossRef](#)] [[PubMed](#)]
15. D0 Collaboration. Observation of the Top Quark. *Phys. Rev. Lett.* **1995**, *74*, 2632. [[CrossRef](#)] [[PubMed](#)]
16. Riess, A.G.; Filippenko, A.V.; Challis, P.; Clocchiatti, A.; Diercks, A.; Garnavich, P.M.; Gilliland, R.L.; Hogan, C.J.; Jha, S.; Kirshner, R.P.; Leibundgut, B.R.U.N.O. [Supernova Search Team]. Observational evidence from supernovae for an accelerating universe and a cosmological constant. *Astron. J.* **1998**, *116*, 1009. [[CrossRef](#)]
17. Perlmutter, S.; Aldering, G.; Goldhaber, G.; Knop, R.A.; Nugent, P.; Castro, P.G.; Deustua, S.; Fabbro, S.; Goobar, A.; Groom, D.E.; Hook, I.M. [Supernova Cosmology Project]. Measurements of Ω and Λ from 42 high redshift supernovae. *Astrophys. J.* **1999**, *517*, 565. [[CrossRef](#)]
18. ATLAS/CMS Dark Matter Forum. Dark Matter benchmark models for early LHC Run-2 Searches: Report of the ATLAS/CMS Dark Matter Forum. *Phys. Dark Univ.* **2020**, *27*, 100371. [[CrossRef](#)]
19. ATLAS Collaboration. Constraints on mediator-based dark matter and scalar dark energy models using $\sqrt{s} = 13$ TeV pp collision data collected by the ATLAS detector. *JHEP* **2019**, *5*, 142.
20. Kamenik, J.F.; Zupan, J. Discovering Dark Matter Through Flavor Violation at the LHC. *Phys. Rev. D* **2011**, *84*, 111502. [[CrossRef](#)]
21. Boucheneb, I.; Cacciapaglia, G.; Deandrea, A.; Fuks, B. Revisiting monotop production at the LHC. *JHEP* **2015**, *1*, 17. [[CrossRef](#)]
22. ATLAS Collaboration. Search for new phenomena in events with same-charge leptons and b -jets in pp collisions at $\sqrt{s} = 13$ TeV with the ATLAS detector. *JHEP* **2018**, *12*, 39.
23. D'Ambrosio, G.; Giudice, G.F.; Isidori, G.; Strumia, A. Minimal flavor violation: An Effective field theory approach. *Nucl. Phys. B* **2002**, *645*, 155. [[CrossRef](#)]
24. Buckley, M.R.; Feld, D.; Goncalves, D. Scalar Simplified Models for Dark Matter. *Phys. Rev. D* **2015**, *91*, 015017. [[CrossRef](#)]
25. Fayet, P. Supersymmetry and weak, electromagnetic and strong interactions. *Phys. Lett. B* **1976**, *64*, 159. [[CrossRef](#)]
26. Fayet, P. Spontaneously broken supersymmetric theories of weak, electromagnetic and strong interactions. *Phys. Lett. B* **1977**, *69*, 489 [[CrossRef](#)]
27. Djouadi, A. The Higgs sector of supersymmetric theories and the implications for high-energy colliders. *Eur. Phys. J. C* **2009**, *59*, 389. [[CrossRef](#)]
28. Particle Data Group. The Review of Particle Physics. *Prog. Theor. Exp. Phys.* **2020**, *2020*, 083C01. [[CrossRef](#)]
29. Carena, M.; Ellis, J.; Lee, J.S.; Pilaftsis, A.; Wagner, C.E. CP Violation in Heavy MSSM Higgs Scenarios. *JHEP* **2016**, *2*, 123. [[CrossRef](#)]
30. Fuchs, E.; Weiglein, G. Impact of CP-violating interference effects on MSSM Higgs searches. *Eur. Phys. J. C* **2018**, *78*, 87. [[CrossRef](#)]
31. Berlin, A.; Lin, T.; Wang, L.T. Mono-Higgs Detection of Dark Matter at the LHC. *JHEP* **2014**, *6*, 078. [[CrossRef](#)]
32. Bauer, M.; Haisch, U.; Kahlhoefer, F. Simplified dark matter models with two Higgs doublets: I. Pseudoscalar mediators. *JHEP* **2017**, *5*, 138. [[CrossRef](#)]
33. Goncalves, D.; Machado, P.A. N.; No, J.M. Simplified Models for Dark Matter Face their Consistent Completions. *Phys. Rev. D* **2017**, *95*, 055027. [[CrossRef](#)]
34. Bell, N.F.; Busoni, G.; Sanderson, I.W. Self-consistent Dark Matter Simplified Models with an s-channel scalar mediator. *JCAP* **2017**, *3*, 15. [[CrossRef](#)]
35. Abe, T.; Fujiwara, M.; Hisano, J. Loop corrections to dark matter direct detection in a pseudoscalar mediator dark matter model. *JHEP* **2019**, *2*, 28. [[CrossRef](#)]
36. Gunion, J.F.; Haber, H. E. The CP conserving two Higgs doublet model: The Approach to the decoupling limit. *Phys. Rev. D* **2003**, *67*, 075019. [[CrossRef](#)]
37. Branco, G.C.; Ferreira, P.M.; Lavoura, L.; Rebelo, M.N.; Sher, M.; Silva, J.P. Theory and phenomenology of two-Higgs-doublet models. *Phys. Rept.* **2012**, *516*, 1. [[CrossRef](#)]

38. LHC Dark Matter Working Group. LHC Dark Matter Working Group: Next-generation spin-0 dark matter models. *Phys. Dark Univ.* **2020**, *27*, 100351. [[CrossRef](#)]
39. ATLAS Collaboration. ATLAS-CONF-2021-036. Available online: <https://atlas.web.cern.ch/Atlas/GROUPS/PHYSICS/CONFNOTES/ATLAS-CONF-2021-036> (accessed on 10 October 2022).
40. Brax, P.; Burrage, C.; Englert, C.; Spannowsky, M. LHC Signatures Of Scalar Dark Energy. *Phys. Rev. D* **2016**, *94*, 084054. [[CrossRef](#)]
41. Horndeski, G.W. Second-order scalar-tensor field equations in a four-dimensional space. *Int. J. Theor. Phys.* **1974**, *10*, 363. [[CrossRef](#)]
42. Joyce, A.; Jain, B.; Khoury, J.; Trodden, M. Beyond the Cosmological Standard Model. *Phys. Rept.* **2015**, *568*, 1. [[CrossRef](#)]
43. ATLAS Collaboration. ATLAS-CONF-2022-036. Available online: <https://atlas.web.cern.ch/Atlas/GROUPS/PHYSICS/CONFNOTES/ATLAS-CONF-2022-036/> (accessed on 10 October 2022).
44. CMS Collaboration. Search for dark matter in events with energetic, hadronically decaying top quarks and missing transverse momentum at $\sqrt{s} = 13$ TeV. *JHEP* **2018**, *6*, 027.
45. Cacciari, M.; Salam, G.P.; Soyez, G. The anti- k_t jet clustering algorithm. *JHEP* **2008**, *4*, 63. [[CrossRef](#)]
46. ATLAS Collaboration. Performance of top-quark and W -boson tagging with ATLAS in Run 2 of the LHC. *Eur. Phys. J. C* **2019**, *79*, 375. [[CrossRef](#)]
47. ATLAS Collaboration. ATL-PHYS-PUB-2020-017. Available online: <https://atlas.web.cern.ch/Atlas/GROUPS/PHYSICS/PUBNOTES/ATL-PHYS-PUB-2020-017/> (accessed on 10 October 2022).
48. Chen, T.; Guestrin, C. XGBoost: A Scalable Tree Boosting System Proceedings of the 22nd ACM SIGKDD International Conference on Knowledge Discovery and Data Mining. *KDD* **2016**, *16*, 785.
49. Thaler, J.; Tilburg, K.V. Identifying Boosted Objects with N-subjettiness. *JHEP* **2011**, *3*, 15. [[CrossRef](#)]
50. Larkoski, A.J.; Salam, G.P.; Thaler, J. Energy Correlation Functions for Jet Substructure. *JHEP* **2013**, *6*, 108. [[CrossRef](#)]
51. Moul, I.; Necib, L.; Thaler, J. New Angles on Energy Correlation Functions. *JHEP* **2016**, *12*, 153. [[CrossRef](#)]
52. Hoecker, A.; Speckmayer, P.; Stelzer, J.; Therhaag, J.; Toerne, E.; Voss, H.; Backes, M.; Carli, T.; Cohen, O.; Christov, A.; et al. TMVA—Toolkit for Multivariate Data Analysis. *arXiv* **2007**, arXiv:0703039.
53. ATLAS Collaboration. Search for large missing transverse momentum in association with one top-quark in proton-proton collisions at $\sqrt{s} = 13$ TeV with the ATLAS detector. *JHEP* **2019**, *5*, 41.
54. CMS Collaboration. Search for dark matter produced in association with a single top quark or a top quark pair in proton-proton collisions at $\sqrt{s} = 13$ TeV. *JHEP* **2019**, *3*, 141.
55. ATLAS Collaboration. Search for dark matter produced in association with a single top quark in $\sqrt{s} = 13$ TeV pp collisions with the ATLAS detector. *Eur. Phys. J. C* **2021**, *81*, 860.
56. ATLAS Collaboration. ATLAS-CONF-2022-012. Available online: <https://atlas.web.cern.ch/Atlas/GROUPS/PHYSICS/CONFNOTES/ATLAS-CONF-2022-012/> (accessed on 10 October 2022).
57. CMS Collaboration. Combined searches for the production of supersymmetric top quark partners in proton-proton collisions at $\sqrt{s} = 13$ TeV. *Eur. Phys. J. C* **2021**, *81*, 970. [[CrossRef](#)]
58. CMS Collaboration. Search for top squark production in fully-hadronic final states in proton-proton collisions at $s = 13$ TeV. *Phys. Rev. D* **2021**, *104*, 052001. [[CrossRef](#)]
59. CMS Collaboration. Search for direct top squark pair production in events with one lepton, jets, and missing transverse momentum at 13 TeV with the CMS experiment. *JHEP* **2020**, *5*, 32.
60. CMS Collaboration. Search for top squark pair production using dilepton final states in pp collision data collected at $\sqrt{s} = 13$ TeV. *Eur. Phys. J. C* **2021**, *81*, 3. [[CrossRef](#)]
61. CMS Collaboration. Identification of heavy, energetic, hadronically decaying particles using machine-learning techniques. *JINST* **2020**, *15*, P06005. [[CrossRef](#)]
62. CMS Collaboration. Performance of missing transverse momentum reconstruction in proton-proton collisions at $\sqrt{s} = 13$ TeV using the CMS detector. *JINST* **2019**, *14*, P07004. [[CrossRef](#)]
63. CMS Collaboration. Search for top squarks and dark matter particles in opposite-charge dilepton final states at $\sqrt{s} = 13$ TeV. *Phys. Rev. D* **2018**, *97*, 032009. [[CrossRef](#)]
64. ATLAS Collaboration. Search for a scalar partner of the top quark in the all-hadronic $t\bar{t}$ plus missing transverse momentum final state at $\sqrt{s} = 13$ TeV with the ATLAS detector. *Eur. Phys. J. C* **2020**, *80*, 737.
65. ATLAS Collaboration. Search for new phenomena with top quark pairs in final states with one lepton, jets, and missing transverse momentum in pp collisions at $\sqrt{s} = 13$ TeV with the ATLAS detector. *JHEP* **2021**, *4*, 174.
66. ATLAS Collaboration. Search for new phenomena in events with two opposite-charge leptons, jets and missing transverse momentum in pp collisions at $\sqrt{s} = 13$ TeV with the ATLAS detector. *JHEP* **2021**, *4*, 165.
67. ATLAS Collaboration. Constraints on spin-0 dark matter mediators and invisible Higgs decays using ATLAS 13 TeV pp collision data with two top quarks and missing transverse momentum in the final state. *arXiv* **2022**, arXiv:2211.05426.
68. ATLAS Collaboration. Search for $t\bar{t}$ resonances in fully hadronic final states in pp collisions at $\sqrt{s} = 13$ TeV with the ATLAS detector. *JHEP* **2020**, *10*, 061.
69. ATLAS Collaboration. Search for heavy particles decaying into top-quark pairs using lepton-plus-jets events in proton-proton collisions at $\sqrt{s} = 13$ TeV with the ATLAS detector. *Eur. Phys. J. C* **2018**, *78*, 565. [[CrossRef](#)] [[PubMed](#)]
70. CMS Collaboration. Search for resonant $t\bar{t}$ production in proton-proton collisions at $\sqrt{s} = 13$ TeV. *JHEP* **2019**, *4*, 31.

71. ATLAS Collaboration. Search for Heavy Higgs Bosons A/H Decaying to a Top Quark Pair in pp Collisions at $\sqrt{s} = 8$ TeV with the ATLAS Detector. *Phys. Rev. Lett.* **2017**, *119*, 191803. [[CrossRef](#)]
72. CMS Collaboration. Search for heavy Higgs bosons decaying to a top quark pair in proton-proton collisions at $\sqrt{s} = 13$ TeV. *JHEP* **2020**, *4*, 171.
73. ATLAS Collaboration. Evidence for $t\bar{t}\bar{t}$ production in the multilepton final state in proton-proton collisions at $\sqrt{s} = 13$ TeV with the ATLAS detector. *Eur. Phys. J. C* **2020**, *80*, 1085.
74. ATLAS Collaboration. Search for $t\bar{t}H/A \rightarrow t\bar{t}\bar{t}$ production in the multilepton final state in proton-proton collisions at $\sqrt{s} = 13$ TeV with the ATLAS detector. *arXiv* **2022**, arXiv:2211.01136.
75. Baldi, P.; Cranmer, K.; Faucett, T.; Sadowski, P.; Whiteson, D. Parameterized neural networks for high-energy physics. *Eur. Phys. J. C* **2016**, *76*, 235. [[CrossRef](#)]
76. ATLAS Collaboration. ATL-PHYS-PUB-2022-036. Available online: <https://atlas.web.cern.ch/Atlas/GROUPS/PHYSICS/PUBNOTES/ATL-PHYS-PUB-2022-036/> (accessed on 10 October 2022).
77. ATLAS Collaboration. Search for new phenomena in a lepton plus high jet multiplicity final state with the ATLAS experiment using $\sqrt{s} = 13$ TeV proton-proton collision data. *JHEP* **2017**, *9*, 088.
78. CMS Collaboration. Search for production of four top quarks in final states with same-sign or multiple leptons in proton-proton collisions at $\sqrt{s} = 13$ TeV. *Eur. Phys. J. C* **2020**, *80*, 75. [[CrossRef](#)]
79. ATLAS Collaboration. ATLAS-CONF-2021-048. Available online: <https://atlas.web.cern.ch/Atlas/GROUPS/PHYSICS/CONFNOTES/ATLAS-CONF-2021-048/> (accessed on 10 October 2022).
80. ATLAS Collaboration. Search for charged Higgs bosons decaying into a top quark and a bottom quark at $\sqrt{s} = 13$ TeV with the ATLAS detector. *JHEP* **2021**, *6*, 145.
81. ATLAS Collaboration. ATLAS-CONF-2022-008. Available online: <https://atlas.web.cern.ch/Atlas/GROUPS/PHYSICS/CONFNOTES/ATLAS-CONF-2022-008/> (accessed on 10 October 2022).
82. CMS Collaboration. Search for charged Higgs bosons decaying into a top and a bottom quark in the all-jet final state of pp collisions at $s \sqrt{s} = 13$ TeV. *JHEP* **2020**, *7*, 126.
83. CMS Collaboration. Search for a charged Higgs boson decaying into top and bottom quarks in events with electrons or muons in proton-proton collisions at $s \sqrt{s} = 13$ TeV. *JHEP* **2020**, *1*, 096.
84. CMS Collaboration. CMS Exotica Summary Plots for 13 TeV Data. Available online: https://twiki.cern.ch/twiki/bin/view/CMSPublic/SummaryPlotsEXO13TeV#DM_summary_plots
85. CMS Collaboration. Search for new particles in events with energetic jets and large missing transverse momentum in proton-proton collisions at $\sqrt{s} = 13$ TeV. *JHEP* **2021**, *11*, 153.
86. CMS Collaboration. Search for low mass vector resonances decaying into quark-antiquark pairs in proton-proton collisions at $\sqrt{s} = 13$ TeV. *Phys. Rev. D* **2019**, *100*, 11.
87. CMS Collaboration. Search for high mass dijet resonances with a new background prediction method in proton-proton collisions at $\sqrt{s} = 13$ TeV. *JHEP* **2020**, *5*, 033.
88. Boveia, A.; Buchmueller, O.; Busoni, G.; D'Eramo, F.; De Roeck, A.; De Simone, A.; Doglioni, C.; Dolan, M.J.; Genest, M.-H.; Hahn, K.; et al. Recommendations on presenting LHC searches for missing transverse energy signals using simplified ss -channel models of dark matter. *Phys. Dark Univ.* **2020**, *27*, 100365. [[CrossRef](#)]
89. Haisch, U.; Polesello, G. Searching for production of dark matter in association with top quarks at the LHC. *J. High Energy Phys.* **2019**, *2019*, 29. [[CrossRef](#)]
90. Pani, P.; Polesello, G. Dark matter production in association with a single top-quark at the LHC in a two-Higgs-doublet model with a pseudoscalar mediator. *Phys. Dark Univ.* **2018**, *21*, 8. [[CrossRef](#)]
91. Pinna, D.; Zucchetta, A.; Buckley, M.R.; Canelli, F. Single top quarks and dark matter. *Phys. Rev. D* **2017**, *96*, 035031. [[CrossRef](#)]
92. Gavela, M.B.; Parga, N. Ward identities and the physical interpretations of anomalies in stochastic quantization. *Phys. Lett. B* **1986**, *169*, 73. [[CrossRef](#)]
93. Choi, K.; Kang, K.; Kim, J.E. Effects of η' in low-energy axion physics. *Phys. Lett. B* **1986**, *181*, 145–149. [[CrossRef](#)]
94. Gavela, M.B.; No, J.M.; Sanz, V.; de Trocóniz, J.F. Nonresonant Searches for Axionlike Particles at the LHC. *Phys. Rev. Lett.* **2020**, *124*, 051802. [[CrossRef](#)]
95. CMS Collaboration. Search for heavy resonances decaying to ZZ or ZW and axion-like particles mediating nonresonant ZZ or ZH production at $\sqrt{s} = 13$ TeV. *JHEP* **2022**, *4*, 87.
96. Carra, S.; Goumarre, V.; Gupta, R.; Heim, S.; Heinemann, B.; Kuchler, J.; Meloni, F.; Quilez, P.; Yap, Y.C. Constraining off-shell production of axionlike particles with $Z\gamma$ and WW differential cross-section measurements. *Phys. Rev. D* **2021**, *104*, 092005. [[CrossRef](#)]
97. Bonilla, J. Available online: <https://ep-news.web.cern.ch/content/non-resonant-searches-open-new-avenues-hunt-axion-particles> (accessed on 10 October 2022).
98. Carmona, A.; Elahi, F.; Scherb, C.; Schwaller, P. The ALPs from the top: searching for long lived axion-like particles from exotic top decays. *J. High Energy Phys.* **2022**, *2022*, 122. [[CrossRef](#)]
99. Brivio, I.; Gavela, M.B.; Merlo, L.; Mimasu, K.; No, J.M.; Del Rey, R.; Sanz, V. ALPs Effective Field Theory and Collider Signatures. *Eur. Phys. J. C* **2017**, *77*, 572. [[CrossRef](#)]
100. Renner, S.; Schwaller, P. A flavoured dark sector. *J. High Energy Phys.* **2018**, *2018*, 052. [[CrossRef](#)]

101. Froggatt, C.; Nielsen, H.B. Hierarchy of Quark Masses, Cabibbo Angles and CP Violation. *Nucl. Phys. B* **1979**, *147*, 277. [[CrossRef](#)]
102. Haisch, U.; Polesello, G.; Schulte, S. Searching for pseudo Nambu-Goldstone boson dark matter production in association with top quarks. *JHEP* **2021**, *9*, 206. [[CrossRef](#)]
103. Kribs, G.D.; Martin, A.; Ostdiek, B.; Tong, T. Dark Mesons at the LHC. *JHEP* **2019**, *7*, 133. [[CrossRef](#)]
104. Dainese, A.; Mangano, M.; Meyer, A.B.; Nisati, A.; Salam, G.; Vesterinen, M.A. Report on the Physics at the HL-LHC, and Perspectives for the HE-LHC. CERN-2019-007. Available online: <https://cds.cern.ch/record/2703572> (accessed on 10 October 2022).
105. Benedikt, M.; Capeans G.M.; Cerutti, F.; Goddard, B.; Gutleber, J.; Jimenez, J.M.; Mangano, M.; Mertens, V.; Osborne, J.A.; Otto, T. FCC-hh: The Hadron Collider: Future Circular Collider Conceptual Design Report Volume 3. Future Circular Collider. CERN-ACC-2018-0058. Available online: <https://cds.cern.ch/record/2651300> (accessed on 10 October 2022).
106. Dutta, B.; Kamon, T.; Ko, P.; Li, J. Prospects for discovery and spin discrimination of dark matter in Higgs portal DM models and their extensions at 100 TeV *pp* collider. *Eur. Phys. J. C* **2018**, *78*, 595. [[CrossRef](#)]
107. Harris, P. Prospects for Discovery and Spin Discrimination of Dark Matter in Higgs Portal DM Models and Their Extensions at 100 TeV *pp* Collider. Talk at FCC Week 2017. Available online: https://indico.cern.ch/event/556692/contributions/2592531/attachments/1469109/2272523/PCH_FCC_DM_v2.pdf (accessed on 10 October 2022).
108. Behnke, T.; James, E. B.; Brian, F.; Juan, F.; Mike, H.; James, M.E.P.; Michael P.; Marcel, S.; Nicholas, W.; Hitoshi, Y. The International Linear Collider Technical Design Report—Volume 1: Executive Summary. *arXiv* **2013**, arXiv:1306.6327.
109. Aicheler, M.; Burrows, P.; Draper, M.; Garvey, T.; Lebrun, P.; Peach, K.; Phinney, N.; Schmickler, H.; Schulte, D.; Toge, N. A Multi-TeV Linear Collider Based on CLIC Technology: CLIC Conceptual Design Report. CERN Yellow Reports: Monographs 2012. Available online: <https://cds.cern.ch/record/1500095> (accessed on 10 October 2022).
110. Linssen, L.; Miyamoto, A.; Stanitzki, M.; Weerts, H. Physics and Detectors at CLIC: CLIC Conceptual Design Report. *arXiv* **2012**, arXiv:1202.5940.
111. The FCC Collaboration. FCC Physics Opportunities. *Eur. Phys. J. C* **2019**, *79*, 474. [[CrossRef](#)]
112. The FCC Collaboration. FCC—The lepton collider. *Eur. Phys. J. S. T.* **2019**, *228*, 261.
113. CEPC Study Group. CEPC Conceptual Design Report: Volume 1—Accelerator. *arXiv* **2018**, arXiv:1809.00285.
114. CEPC Study Group. CEPC Conceptual Design Report: Volume 2—Physics & Detector. *arXiv* **2018**, arXiv:1811.10545.

Disclaimer/Publisher’s Note: The statements, opinions and data contained in all publications are solely those of the individual author(s) and contributor(s) and not of MDPI and/or the editor(s). MDPI and/or the editor(s) disclaim responsibility for any injury to people or property resulting from any ideas, methods, instructions or products referred to in the content.